

Observations of Facet Formation in Near- α Titanium and Comments on the Role of Hydrogen

A.L. PILCHAK and J.C. WILLIAMS

Faceted features are frequently observed on the fracture surfaces of titanium alloys that have failed by static loading, continuous cycling, dwell fatigue loading, and stress corrosion cracking (SCC). Although the facets formed under different loading conditions seem qualitatively similar, there are significant differences in the spatial and crystallographic orientations of the facets as well as subtle differences in facet surface topography. The current study compares and contrasts facets for various loading conditions (cyclic, creep, SCC, and dwell) in the Ti-8Al-1Mo-1V alloy with the primary motivation being to understand the mechanisms of crack initiation and faceted growth during dwell fatigue. The spatial and crystallographic orientations of the facets were determined using quantitative tilt fractography and electron backscatter diffraction, whereas facet topography was examined using ultra-high-resolution scanning electron microscopy. Collectively, the experimental observations suggest that hydrogen may play an important role in facet formation and accelerating small crack growth rates during dwell fatigue loading.

DOI: 10.1007/s11661-010-0507-9

© The Minerals, Metals & Materials Society and ASM International 2010

I. INTRODUCTION

BASED on experimental observations over the past several decades, there is a basic understanding of the sequence of fatigue crack formation during continuous cycling. Many researchers have observed first the formation of planar slip bands, followed by crack initiation and propagation along these slip bands.^[1-3] On the fracture surface, cracking along a slip band leads to the formation of planar features that are commonly referred to as facets.^[4] In addition to being present on failures resulting from continuous cycling, facets are also characteristic of the fracture surfaces near the origin areas of specimens that have failed by dwell fatigue,^[5-7] static loading in air,^[8,9] and stress corrosion cracking.^[10,11] Among these, there has been considerable controversy surrounding the origins and characteristics of facets found on dwell fatigue specimens.

Dwell fatigue failures created in the laboratory and occurring in service are generally characterized as having subsurface crack-initiation sites with planar facets that can be either inclined or nearly perpendicular to the loading direction depending on the magnitude of applied stress.^[6,8,12] Furthermore, dwell fatigue facets have been generalized widely as being “on or near” the basal plane.^[6,12-15] Early work by Evans^[12] suggested

that the facet planes were oriented within 5 deg of the basal plane, and were also nearly perpendicular to the loading direction. Thus, it became necessary to rationalize how slip could occur on basal planes that were oriented nearly perpendicular to the loading direction that had essentially zero resolved shear stress. Consequently, Evans and Bache^[6] proposed a conceptual model based on Stroh’s formulation of the stress field around a dislocation pileup in an isotropic material and subsequent crack nucleation from this pileup. This model is shown schematically in Figure 1.

The authors contended that at low applied stress levels, only the most suitably oriented grains with slip planes inclined to the loading direction would be able to accumulate strain by dislocation slip (the “soft grain”). The so-called source slip band is blocked by a grain boundary such that a dislocation pileup forms. The dislocation pileup that forms on the source slip band induces a normal stress and a shear stress field that is resolved onto the basal plane of the adjacent grain (the “hard grain”). The magnitude of the resolved stress depends primarily on the angle between the source slip band and the slip plane in the adjacent grain as well as the available slip length (which determines the maximum pileup length) in the soft grain. In the Evans and Bache^[6] adaptation of Stroh’s original model, it was suggested that the shear stress induced by the pileup in the soft grain provided sufficient shear stress onto the basal plane of the hard grain such that slip could occur. Additionally, the resolved normal stress would combine with the far field applied stress to cause decohesion of the slip band on the (0001) plane of the hard grain resulting in facet formation along the slip band.

The Stroh-like model proposed by Evans and Bache,^[6] although it is conceptually useful for understanding some experimental observations, it does not explain the time dependent nature of dwell fatigue, nor

A.L. PILCHAK, formerly Graduate Research Associate, Department of Materials Science and Engineering, The Ohio State University, Columbus, OH 43210, is now Visiting Scientist, Air Force Research Laboratory, Materials and Manufacturing Directorate, Metals Processing Group, Wright Patterson Air Force Base, OH 45432 and Research Scientist, Universal Technology Corporation, Dayton, OH 45433. Contact e-mail: adam.pilchak@wpafb.af.mil J.C. WILLIAMS, Professor and Honda Chair Emeritus, is with the Department of Materials Science and Engineering, The Ohio State University.

Manuscript submitted April 2, 2010.

Report Documentation Page

Form Approved
OMB No. 0704-0188

Public reporting burden for the collection of information is estimated to average 1 hour per response, including the time for reviewing instructions, searching existing data sources, gathering and maintaining the data needed, and completing and reviewing the collection of information. Send comments regarding this burden estimate or any other aspect of this collection of information, including suggestions for reducing this burden, to Washington Headquarters Services, Directorate for Information Operations and Reports, 1215 Jefferson Davis Highway, Suite 1204, Arlington VA 22202-4302. Respondents should be aware that notwithstanding any other provision of law, no person shall be subject to a penalty for failing to comply with a collection of information if it does not display a currently valid OMB control number.

1. REPORT DATE OCT 2010		2. REPORT TYPE		3. DATES COVERED 00-00-2010 to 00-00-2010	
4. TITLE AND SUBTITLE Observations of Facet Formation in Near-a Titanium and Comments on the Role of Hydrogen				5a. CONTRACT NUMBER	
				5b. GRANT NUMBER	
				5c. PROGRAM ELEMENT NUMBER	
6. AUTHOR(S)				5d. PROJECT NUMBER	
				5e. TASK NUMBER	
				5f. WORK UNIT NUMBER	
7. PERFORMING ORGANIZATION NAME(S) AND ADDRESS(ES) Air Force Research laboratory, Materials and Manufacturing Directorate, Metals Processing Group, Wright Patterson AFB, OH, 45432				8. PERFORMING ORGANIZATION REPORT NUMBER	
9. SPONSORING/MONITORING AGENCY NAME(S) AND ADDRESS(ES)				10. SPONSOR/MONITOR'S ACRONYM(S)	
				11. SPONSOR/MONITOR'S REPORT NUMBER(S)	
12. DISTRIBUTION/AVAILABILITY STATEMENT Approved for public release; distribution unlimited					
13. SUPPLEMENTARY NOTES					
14. ABSTRACT					
15. SUBJECT TERMS					
16. SECURITY CLASSIFICATION OF:			17. LIMITATION OF ABSTRACT	18. NUMBER OF PAGES	19a. NAME OF RESPONSIBLE PERSON
a. REPORT unclassified	b. ABSTRACT unclassified	c. THIS PAGE unclassified			

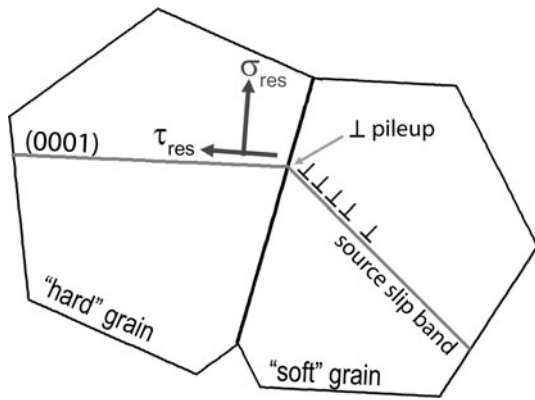


Fig. 1—Schematic representation of the Stroh model as modified by Evans and Bache^[6] for dwell fatigue.

incorporate the anisotropic elasticity or plasticity of the α phase. Furthermore, the model is based on the assumption that the crack initiates on the basal plane of the hard grain, which is orthogonal to the loading direction and that slip is necessary for this to occur. The requirement that slip precedes facet formation, however, has not been experimentally demonstrated satisfactorily. In fact, there was evidence as early as 1980^[16] that dwell facet fracture planes were not coincident with the basal plane. Davidson and Eylon^[16] used selected area electron channeling to determine the crystallographic plane of fracture to an accuracy of ± 3 deg in continuously cycled and dwell fatigued IMI-685. The authors also made a distinction between those facets near the crack-initiation site and those that were propagation facets. In both locations on the dwell fatigued specimen, the facet planes were consistently oriented between 5 deg and 15 deg from the basal plane, with the larger angular deviations being preferred over the smaller ones in the propagation facet regime. In contrast, the facets on specimens subjected to continuous cycling fractured considerably nearer the basal plane. The initiation facets were reported to be precisely on the basal plane, whereas the propagation facets showed deviations as large as 10 deg from it. However, the angle between the facet normal direction and the loading direction was not reported explicitly for each facet.

Sinha *et al.*^[7,8] have recently supported these measurements using a higher fidelity combined tilt fractography/electron backscatter diffraction (EBSD) technique in which both the crystallographic orientation of the fractured grain and the spatial orientation of the facet are considered for an accurate determination of facet crystallography. Sinha *et al.*^[7,8] examined only propagation facets on specimens of Ti-6Al-2Sn-4Zr-2Mo subjected to continuous cycling, static loading in air, and 2-minute dwell fatigue cycles. The fracture planes of the continuously cycled and dwell specimens were consistent with those observed by Davidson and Eylon,^[16] being inclined to (0001) approximately 5 deg and 10 to 15 deg, respectively. In addition, the analysis by Sinha *et al.*^[8] showed that the fracture plane of facets formed during static loading deviated approximately

15 to 20 deg from (0001). More recently, Uta *et al.*^[17] have also reported deviations between 10 and 20 deg from the basal plane on dwell fatigue crack propagation facets in IMI834 after accounting for their spatial orientation. In contrast, the authors reported that the initiation facets on dwell fatigue specimens were more nearly coincident with the basal plane. Unfortunately, the spatial orientations were not reported explicitly for the initiation or propagation facets.

In the current study, we have analyzed the spatial and crystallographic orientations of initiation and propagation facets formed by continuous cycling, static loading both in air and in 3.5 pct NaCl and by dwell fatigue loading. In addition to studying the crystallographic and spatial orientations, we have also used ultra-high-resolution scanning electron microscopy to study the surface topography of the facets to use it along with the crystallographic information to understand the micro-mechanisms of crack initiation and propagation during dwell fatigue.

II. MATERIALS AND EXPERIMENTAL PROCEDURE

A 12.7-cm diameter, 127-cm long Ti-8Al-1Mo-1V bar with ~ 10 ppm hydrogen was provided by Timet (Henderson, NV). Blanks for mechanical test specimens were extracted transverse to the bar axis by wire electrical discharge machining. All the tests were performed on material in the as-received condition. The blanks were machined into round specimens with diameters of either 5.08 mm (cyclic and dwell loading) or 4.06 mm (static loading) with gauge lengths of 19.05 mm and 16.9 mm, respectively. The specimens were tested under four different loading conditions: continuous cycling at 30 Hz, 2-minute dwell periods with 1 second each down- and up-ramp loading, static loading at room temperature in lab air and static loading in 3.5 pct NaCl. All the tests were run in load control, and the peak stress attained during any one test was constant for all tests at 758 MPa, which was 95 pct of the yield strength measured from a tensile test conducted according to ASTM E8 standards. The load ratio was 0.1 for the continuous cycling and dwell tests. The cyclic tests were performed on a servohydraulic test frame that was aligned precisely with a strain gauged standard specimen prior to testing. The stress corrosion and static loading experiments were performed on an M-Cert Test System (InterCorr International, Inc., Houston, TX), which is controlled by a precision step motor. Because Ti-811 exhibits increased susceptibility to stress corrosion cracking in 3.5 pct NaCl in the presence of a notch,^[18] a diamond scribe was used to scratch 1 mm to 2 mm lines arbitrarily around the circumference of the gauge section in several random locations perpendicular to the loading direction.

Microstructure characterization and fractographic investigations were performed with a FEI (FEI Company, Hillsboro, OR) Sirion field emission gun (FEG) scanning electron microscope (SEM), whereas quantitative tilt fractography and EBSD measurements were performed in either an FEI Quanta 200 tungsten

emission source SEM or an FEI XL30 FEG SEM. For imaging purposes, a 30- μm objective aperture was used with accelerating voltages varying between 12 kV and 20 kV and spot sizes of either 4 or 5. Images were acquired using the secondary electron detector as well as the through-lens detector (TLD) when the Sirion was operated in ultra-high-resolution (UHR) mode. The TLD is a scintillation detector that is mounted inside the pole piece of the SEM. In this configuration, the electrons used to create the image must pass through the pole piece to return to the detector so only the highest energy electrons are collected. This detector can be biased either positively or negatively to collect secondary or backscattered electrons, respectively. A positive bias of 20 V was used in the current study. In addition, selecting this imaging mode alters the magnetic field in the SEM chamber, which refines the probe size, thereby increasing the resolution of the SEM. In contrast, a larger probe size was desired for the tilt fractography experiments, so a 100- μm objective aperture was used in conjunction with a 20-kV accelerating voltage to produce a high beam current, on the order of 10 nA, to provide as large of a backscattered volume as possible to penetrate surface layers of plastically deformed material. Even under these conditions, the interrogated volume is still small compared with the grain size, and so each pattern collected originates from a single grain.

A. Spatial Orientation and the Crystallographic Plane of Fracture

The technique to characterize fully the faceted initiation sites by determining both the spatial orientation of the facet and the crystallographic plane of fracture has been described previously in detail.^[4,7,8,19] Briefly, the technique involves acquiring images (of the same magnification) of the same location at two different tilt angles and identifying a common origin and three common features in both images. The coordinates of each feature are determined within a fixed-image coordinate system that is chosen to coincide with the reference frame of the EBSD system being used. Using the equations developed by Themelis *et al.*,^[20] the spatial orientation of the facet are used to determine two vectors that lie in the plane of the facet whose cross product defines a unit vector within the sample reference frame that defines the facet normal. An inverse pole figure centered on the facet normal vector containing the orientation of the faceted grain as-measured by EBSD is calculated to determine the crystallographic plane of fracture. Recently, we have also shown that calculating an inverse pole figure with respect to the vectors in the facet plane can also be useful to correlate the local dominant crack growth direction with crystallographic orientation if the vectors are placed strategically in the plane of the facet.^[4] This technique is reported to be accurate between 1 deg^[8] and 3 deg^[21] when the spatial and crystallographic information is collected in the same microscope session without rotating the stage. Thus, in the current work, we have rounded the spatial orientations of the facets with respect to the loading axis to the nearest integer.

III. RESULTS AND DISCUSSION

A. Characterization of As-Received Bar

The microstructure (Figure 2) and texture (Figure 3) of the as-received bar were characterized with scanning electron microscopy and EBSD, respectively. The microstructure was bimodal consisting of a globular α grains approximately 10 μm to 15 μm in diameter with approximately 30 vol pct to 35 vol pct $\alpha + \beta$ colonies. The secondary α was not arranged into well-defined colonies as in classic bimodal microstructures. Instead, it was relatively coarse and in many locations seemed to have multiple variants of α phase. An EBSD analysis has shown that the secondary α has adopted similar basal plane orientation as the adjacent primary α grains in many locations, although this is certainly not a “rule” of the phase transformation. With respect to texture, there was a weak 10 $\bar{1}0$ partial fiber aligned with the bar axis (Figure 3). EBSD scans made on large areas of longitudinal sections that contained the bar axis in the plane of polish revealed that there were elongated regions of similarly oriented grains, or microtextured regions, that had widths ranging between 100 and 500 μm (Figure 4).

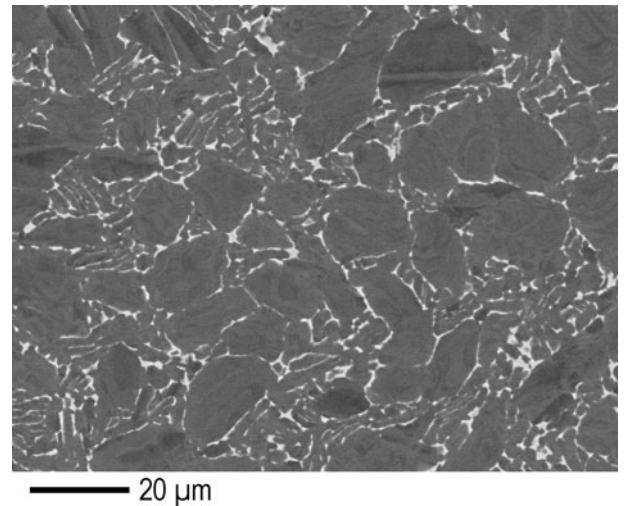


Fig. 2—Microstructure of the as-received Ti-811 bar.

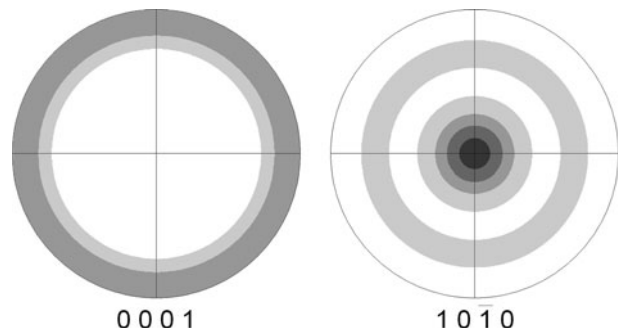


Fig. 3—The texture of the as-received bar indicating the presence of a weak 10 $\bar{1}0$ partial fiber along the bar axis (which is perpendicular to plane of projection). The levels of intensity are in intervals of 0.5 multiples of the probability of a random distribution.

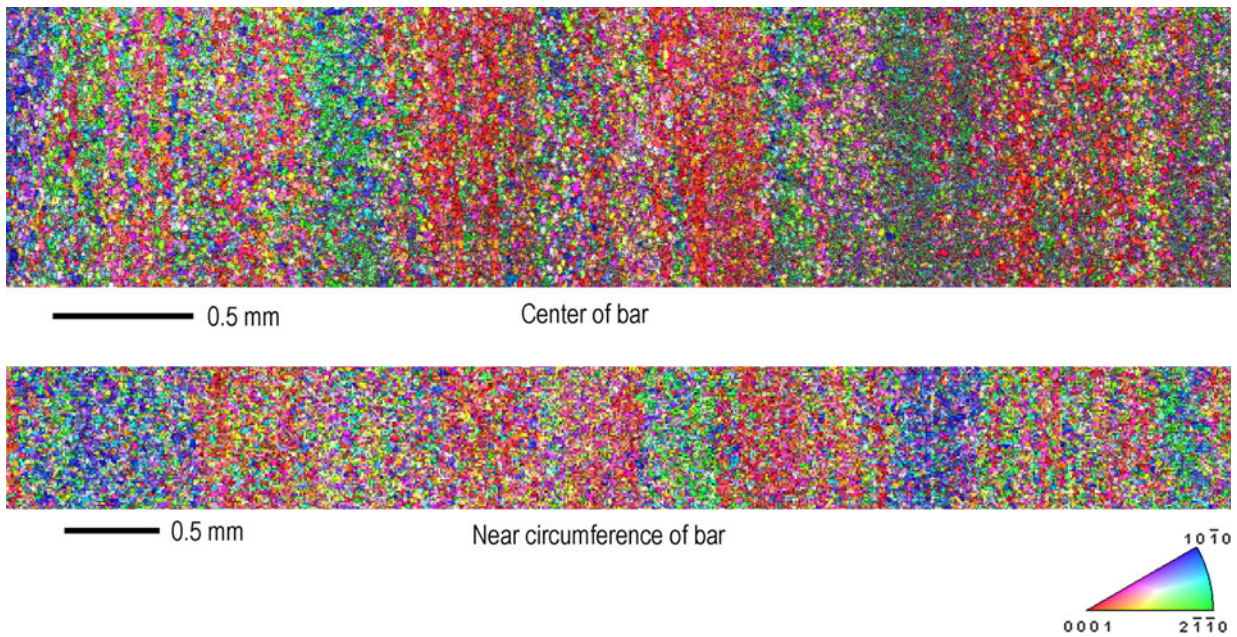


Fig. 4—Normal direction inverse pole figure EBSD maps of longitudinal sections cut from near the center and edge of the bar showing elongated bands of microtexture. The loading direction is perpendicular to the plane of polish. (Color figure online).

Based on these data, specimens were cut transverse to the bar axis. As a consequence of the axial symmetry about the bar axis, there was an equal distribution of basal poles oriented between 0 and 90 deg to the loading direction. Thus, the macroscopic texture of the bar would not influence the orientation of the grain in which crack initiation occurs as it could if there were limited grains in the gauge section or in highly textured plate, for instance.

B. Mechanical Tests

The primary purpose of the current study was to create facets by various testing methods to study their characteristics. As a result, no extensive data acquisition was made during the tests; however, the lives of the fatigue specimens and the time to failure of the static loading experiments reveal some potentially important trends. For instance, the specimen that was cycled continuously at 95 pct of the yield strength failed after 138,840 cycles, whereas the specimen subjected to 2-minute dwell periods at the same fraction of the yield stress failed after only 10,399 cycles, a debit of approximately 13 times. To the authors' knowledge, this is the first time dwell sensitivity has been reported in Ti-811. This alloy has not been investigated previously for dwell sensitivity because it is not an alloy used for jet engine rotors; however, this finding is potentially significant because there are Ti-811 fan blades in service.

With regard to static loading, the specimen loaded in 3.5 pct NaCl failed after 10 hours and 31 minutes at 758 MPa. The specimen statically loaded in air, in the absence of crack initiating notch and an aggressive environment, exhibited significantly longer life. This specimen was loaded for 426 hours at 758 MPa at which

point the load was increased to the macroscopic yield strength, 798 MPa. After the load increase, the specimen failed after an additional 26 hours and 42 minutes.

C. Macroscopic Fracture Surface Analysis

The fracture surfaces were all qualitatively similar in the sense that they contained facets and features, like dimples and shear lips, typically associated with overload failure. The regions between faceted growth and overload fracture were considerably different among the various specimens because of the different loading histories. However, the features from this region are not discussed in this manuscript because of the level of depth in which the facets are addressed. Although all the samples contained facets, the overall size and shape of the faceted regions were different. Secondary electron images of the as-fractured specimens are shown in Figure 5. The fracture surface of the cyclic specimen was typical of a fatigue failure, exhibiting surface crack initiation and a small, semielliptical faceted region near the surface of the specimen. The region of faceted growth transitioned to more conventional striation growth gradually, which is consistent with many observations of cyclic fatigue crack growth.^[22–27] Striations were first observed in isolated grains at crack lengths less than 200 μm and became the dominant propagation mechanism at crack lengths > 1 mm. Striation growth proceeded with the macroscopic fracture plane remaining approximately perpendicular to the loading direction until the critical crack length was reached and overload fracture occurred resulting in the formation of a shear lip.

In contrast, the dwell-fatigued specimen exhibited subsurface crack initiation and had a considerably larger

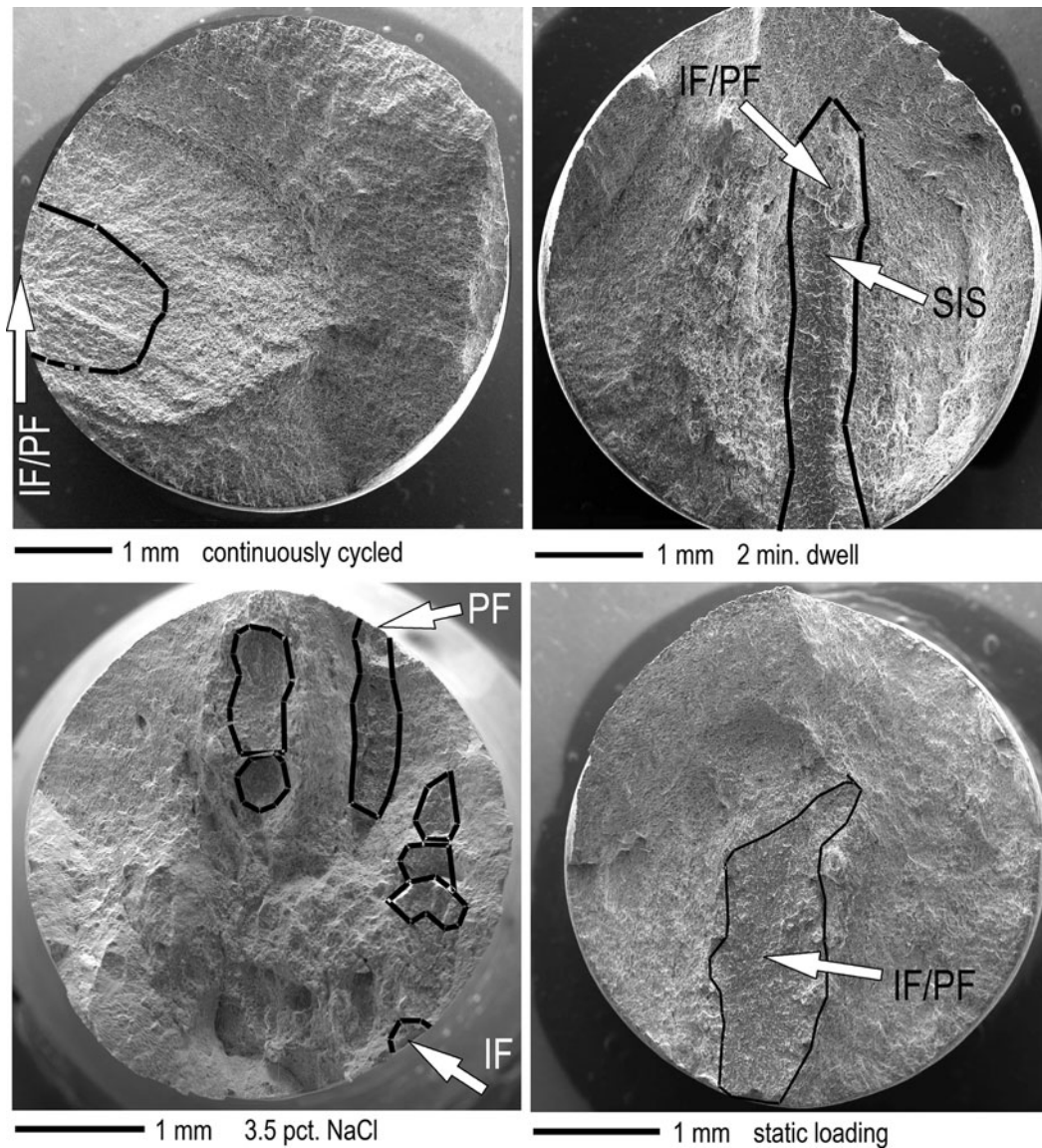


Fig. 5—Low-magnification SEM images of the fractured specimens. The faceted regions on each specimen are enclosed by black lines. The locations of the initiation facets (IF) and propagation facets (PF) discussed in more detail in the text are identified on each fracture surface. The location of a secondary initiation site (SIS) on the dwell fatigue specimen is also shown.

faceted region that was on the order of $250\ \mu\text{m}$ wide and extended approximately 3 mm from the circumference of the specimen into the gauge section. Similar elongated faceted regions were observed on all the statically loaded specimens, suggesting that the formation of such regions is unique to sustained loading. It is noteworthy that the length scale, aspect ratio, and physical orientation of these elongated faceted regions is consistent with that of the microtextured regions observed in the as-received bar material (Figure 4). This correlation has possibly been overlooked in the past because the microtextured regions in the $\alpha + \beta$ forged pancake material analyzed by Sinha *et al.*^[28] were approximately equiaxed in shape. In addition, Sinha *et al.*^[28] did not explicitly identify where in the faceted region the crack started and thus a preferential growth could not be identified. Uta *et al.*^[17] have also studied the fracture surface specimen that

failed during dwell fatigue loading that had elongated bands of microtexture similar to the material studied here. However, the authors used a 30-second dwell period and did not observe such a strong preference for the faceted region to correlate with the underlying microtextured regions.

The specimen statically loaded in air was most similar to the dwell fatigue specimen in the sense that there was subsurface initiation and subsequent formation of an elongated faceted region, and the fracture surface was relatively flat, aside from the shear lip. In contrast to the relatively flat fracture surfaces of the previous specimens, the macroscopic appearance of the specimen that failed by static loading in 3.5 pct NaCl had substantial variations in height among the various locations on the fracture surface. This suggests, as later confirmed by more detailed fractography, that cracks grew inward

from multiple locations at the surface of the sample until the remaining ligaments could no longer support the applied stress and failed by overload fracture. Several cracks entered via faceted growth while other cracks propagated by mechanisms that formed ductile fracture features until encountering a differently oriented microtextured region. It is notable that the crack propagation mechanism changed from ductile to faceted with increasing crack length. This is in stark contrast to fatigue cracks, which typically propagate by faceted growth at small crack lengths and transition to striation growth, and then dimples at longer crack lengths because of the increase in the stress intensity at the crack tip with increasing crack length. This observation suggests that the size of the crack tip plastic zone is not the dominant factor governing fracture topography during SCC as the cyclic crack tip plastic zone is during fatigue. Instead, the local fracture mode seems to be much more strongly dependent on local orientation.

D. Facet Topography, Spatial, and Crystallographic Orientation Analysis

The individual facets within the elongated faceted regions on all the specimens seemed qualitatively similar under relatively low magnifications of 50 times to 100 times. The diameters of the thousands of individual facets that constituted the larger faceted regions described above were consistent with the diameters of the α grains as measured by EBSD and from the backscattered electron micrographs. In addition, some facets were elongated with aspect ratios between 2:1 and 3:1 consistent with metallographic observations made on transverse sections of the as-received material. All the fractured specimens were examined optically and with the SEM. The spatial and crystallographic orientations of several grains were also determined directly from the as-fractured surfaces. Throughout this section, the facets are identified by a prefix describing the loading type,

either cyclic (CY-), dwell (DW-), static (ST-), or stress corrosion cracking (SCC-), followed by an integer.

1. Continuous Cycling

There was a single clearly identifiable fatigue crack-initiation site in the specimen loaded by continuous cycling. This region is shown at two levels of magnification in Figure 5 and Figure 6. Although there was no large, contiguous faceted region consistent with the microtextured regions in this specimen, several facets were observed at the crack-initiation site (Figure 6). Although some of the facets directly bordered one another, there were many locations separated by sharp, planar features such as those identified as numbers 2 and 3 in Figure 6. In the strictest sense, these could be called facets, but we reserve that term for the more planar features identified by the remaining numbers (1, 4, 5, 6, and 7) that are formed by transgranular fracture through a primary α grain with a fracture plane nearer the basal plane than any other low index plane as will be shown in the subsequent sections. Except for the initiation facet, several markings on the facet surfaces were indicative of the local crack propagation direction (Figure 7). Subsequent facet surfaces were observed to be progressively and continuously more rough with increasing crack length. In addition, the number of steps on the facet surfaces seemed to increase in density with each grain boundary encountered by the crack front. For the case of continuous cycling, this is related to the increase in the cyclic crack tip plastic zone size with increasing crack length,^[27] which results in a larger fracture process zone on each subsequent cycle. At high magnifications while using the TLD, striations were occasionally visible on some facets. Two examples are shown in Figure 8 where, on the left, the striations resemble slip steps on the facet surface while, on the right, they resemble more conventional striations. At a crack length of approximately 100 μm , the spacing of these striations was on the order of 150 nm cycle⁻¹.

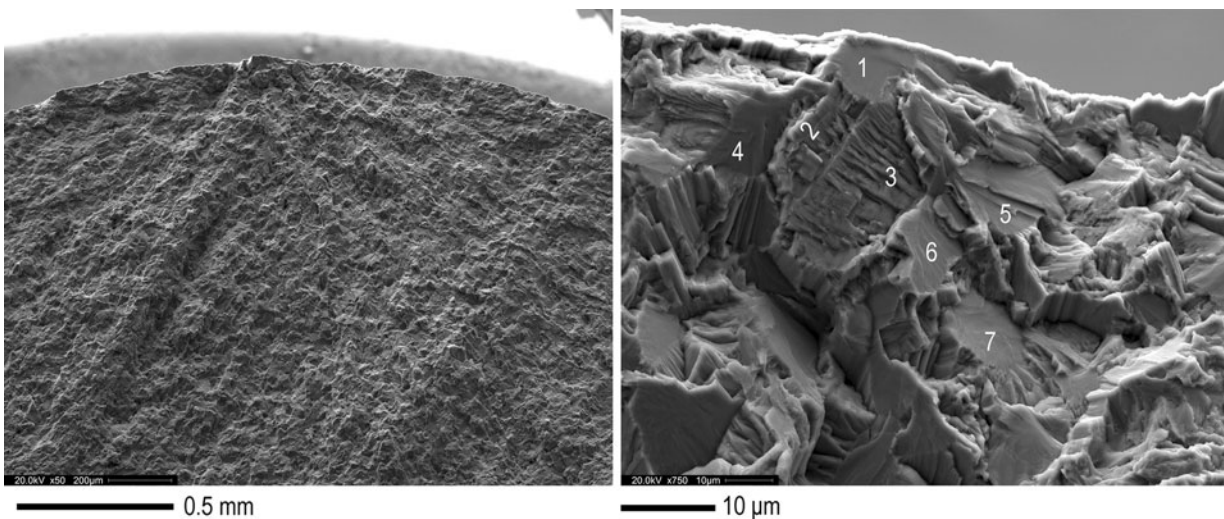


Fig.6—Crack-initiation site in the continuously cycled specimen in the as-received condition. Several facets are identified by numbers 1 through 7 (CY-1 through CY-7).

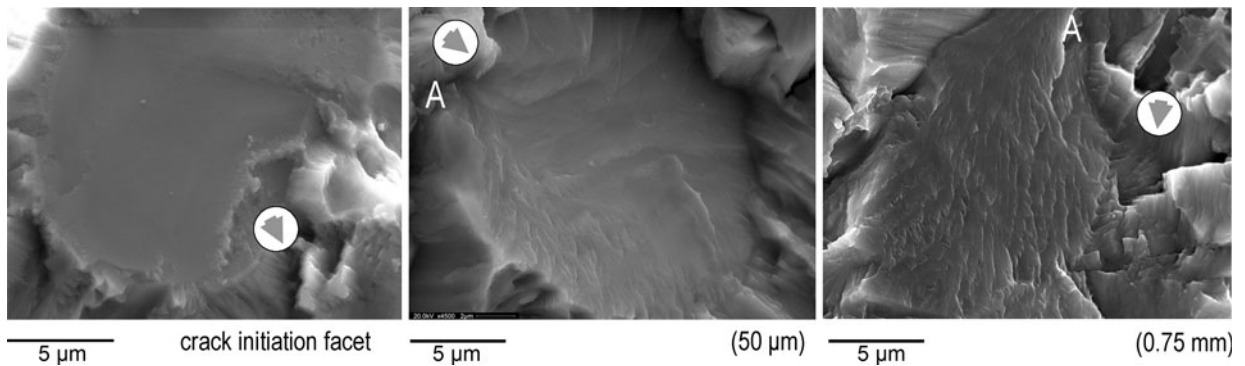


Fig. 7—The effect of crack length on facet topography in the cyclically loaded specimen in the as-received condition. The local crack propagation direction is indicated by the arrows while the letter A designates the point at which the crack entered the grain.

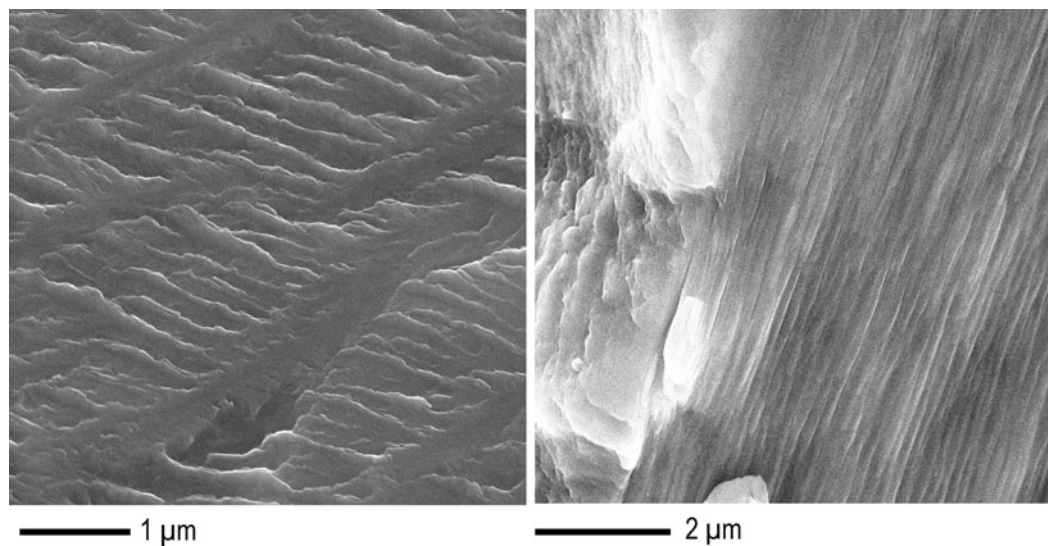


Fig. 8—High-magnification secondary electron images of two different facet surfaces in the continuously cycled specimen at crack lengths $\sim 100 \mu\text{m}$. The markings on the facet surfaces suggest the crack growth rate is on the order of $150 \text{ nm cycle}^{-1}$.

The spatial and crystallographic orientations of all the facets identified in Figure 6 (except for CY-7) were determined using the combined EBSD/quantitative tilt fractography technique. The results have been compiled in Figure 9, which shows the orientations of each fractured grain with respect to the loading direction and also with respect to the facet normal direction. A total of seven individual EBSD patterns were collected and indexed from the first grain to fracture (CY-1), whereas two patterns were collected from the remaining grains. Initiation occurred within a primary α grain that had its c -axis oriented 24 deg from the loading direction. The angle between the facet normal and the loading direction was 27 deg, and the fracture plane was determined as being parallel to the basal plane for all seven indexed patterns within the resolution of the technique. The spatial and crystallographic orientations of this primary α grain initiation site are consistent with observations made on fatigue crack-initiation facets in α grains in continuously cycled Ti-6Al-4V^[29,30] and Ti-6246^[31,32] specimens with bimodal microstructures. In addition, despite being near the surface of the specimen,

the orientation of this grain is such that it could not have formed a slip band extrusion on the surface of the specimen as the only available $\langle a \rangle$ slip system, which could intersect the specimen surface had the lowest resolved shear stress. Thus, in this case, crack initiation seems to be the result of grain-to-grain interactions and not classic surface intrusion/extrusion.

Two grains (CY-2 and CY-3) directly adjacent to the crack initiating grain have their c axes nearly perpendicular to the applied loading direction. In this orientation, the maximum resolved shear stress is on the prismatic $\langle a \rangle$ slip systems, and there is nearly zero resolved shear stress on the basal plane. Whereas there are also suitably oriented $\langle c + a \rangle$ slip systems, the higher critical resolved shear stress of these systems^[33] implies that the grains would tend to deform by prismatic $\langle a \rangle$ slip. Because these two grains did not fracture on a flat, continuous faceted plane, the average fracture plane was determined over several areas spanning $\sim 8 \mu\text{m}$ each on the fracture surface. After correcting for this average fracture plane normal, the plane of fracture was determined to be near $\{10\bar{1}0\}$ for CY-2 and

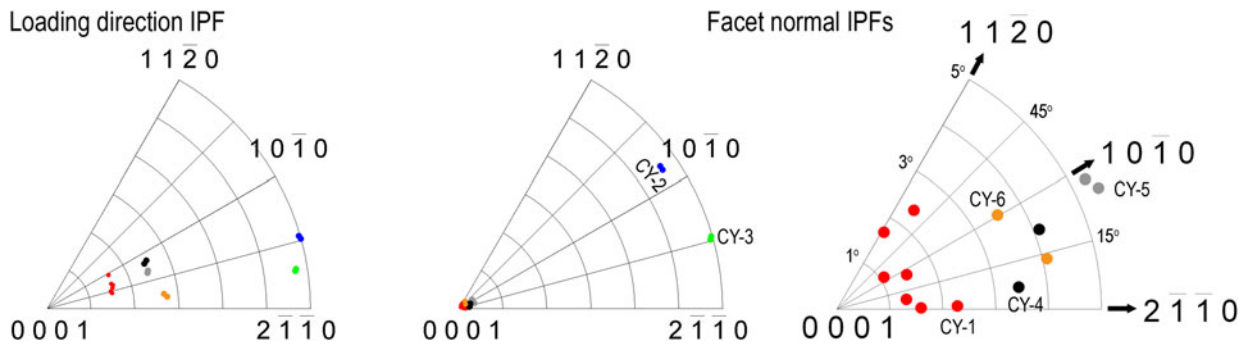


Fig. 9—Results from the facet crystallography analysis on the continuously cycled fatigue specimen. The IPF on the right is a magnified view of the region around 0001 in the center facet normal IPF (also note the change in scale for this IPF). (Color figure online).

$\{72\bar{5}0\}$ (parallel to the α/β interface) for CY-3. The average fracture plane normal for these regions was determined to be 41 deg (CY-2) and 25 deg (CY-3). The size, appearance, and spatial orientation of these regions are consistent with the underlying microstructure being transformed β based on previous work conducted on bimodal Ti-6Al-4V, in which there was direct observation of the fracture surface and the underlying microstructure.^[30]

The remaining facets, CY-4 through CY-6, can be characterized as transgranular propagation facets through primary α grains. These facet normal directions made angles (in order) of 36 deg, 40 deg, and 44 deg with the loading direction. The crystallographic plane of fracture was near the basal plane for all facets; however, there was a slight deviation from the basal plane observed for all specimens with facet CY-5 being the furthest, at an angle \sim 5 deg. It is believed that these discrepancies can be attributed to errors introduced to the spatial orientation calculation by the increased facet surface roughness and the formation of steps as discussed in depth by Pilchak *et al.*^[27] Thus, these grains are all in orientations that could have easily formed a slip band on the basal plane followed by cracking along that slip band.

The transformed β regions adjacent to the primary crack-initiation facet were in elastically and plastically soft orientations. The crack-initiating grain was in neither a hard nor a soft orientation, as it was capable of slip on the basal plane. However, the spatial orientation of the facet also resulted in a considerable resolved normal stress on the facet plane, which has been suggested as being necessary for crack nucleation during continuous cycling fatigue of Ti-8Al-1Mo-1V.^[2] It is likely that crack initiation occurs in the primary α constituents because of the elemental partitioning effect, which results in higher Al content in this constituent during elevated temperature thermomechanical processing. Thus, it is more prone to planar slip^[33] than the transformed β regions, which also have many α/β interfaces that can form pileups under certain circumstances,^[34,35] which can presumably result in delayed crack initiation.^[4] However, the definition of a detailed, mechanism-based understanding of the crack nucleation process for the continuously cycled specimen tested here is still unclear.

It is clear, however, that the initiation mechanism is not the result of a classic cleavage mechanism. The crack-initiation facet is inclined to the loading direction and has formed on a plane in which slip has occurred previously. Furthermore, spectrum loading experiments^[22,27] have shown conclusively that facets do not form during a single load cycle during continuous cycling but rather that the crack tip advances incrementally, cycle by cycle through each individual grain. Then, depending on the details of the local grain boundary structure, there might be an incubation period^[36] before the crack begins to propagate into the next grain. The incubation period would be governed by microstructural factors such as crystallographic misorientation, grain boundary orientation, and the degree of coplanarity between the current crack plane and the preferred crack propagation plane in the adjacent grain. Because this is a plasticity-controlled growth mechanism, the local stress intensity range would be the dominant factor driving crack extension as opposed to exceeding a critical normal stress as in classic cleavage.

Subsequent faceted propagation occurred through nearby primary α grains that were also inclined to the loading direction. As shown in the inverse pole figures (Figure 9), seven EBSD patterns were collected from the crack-initiation facet (CY-1) along a horizontal line spanning the diameter of the facet. Although the data seem to be noisy, when plotted on 0001 and 1020 equal angle projections as shown in Figure 10(a), it is evident that collectively these patterns reveal a continuous lattice rotation about [0001] of approximately 10 deg. Although it is tempting to relate this to the facet formation process, high-resolution EBSD analysis of the as-received material indicated that similar lattice rotations were present within the primary α grains (Figure 10(b) and (c)). It is noteworthy that a similar analysis of facets formed during cyclic loading of well-annealed material (with no residual dislocation content) produced similar facet surface features on both initiation and propagation facets. Thus, the presence of residual stored work does not seem to influence fracture topography.

2. Static Loading in Air

It was considerably more difficult to locate the crack-initiation site in the specimen statically loaded in air

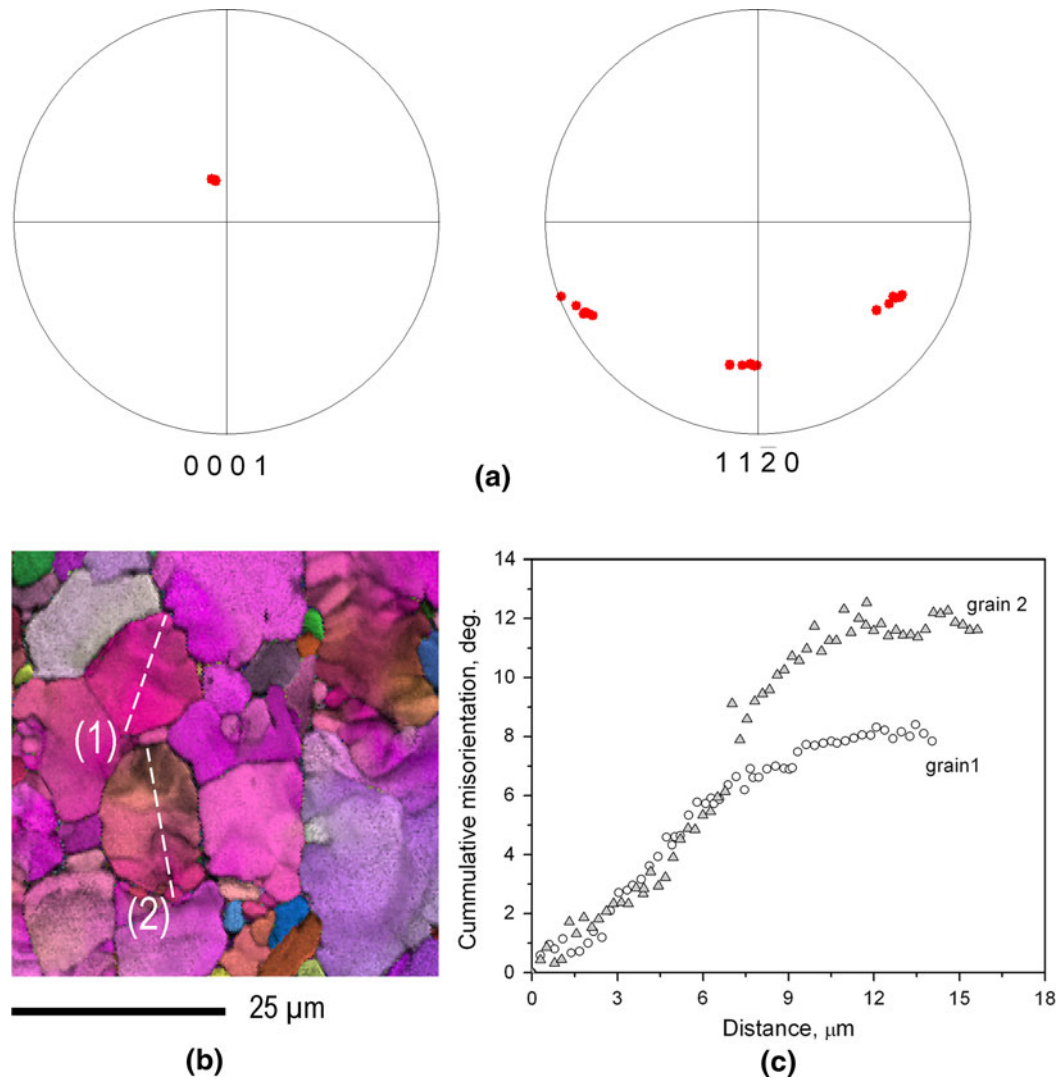


Fig. 10—(a) 0001 and $11\bar{2}0$ equal-area-projection pole figures showing all of the orientations indexed from the crack-initiation facet (CY-1) in the continuously cycled specimen. The basal pole remains in the same position; however, there is a rotation of 10 deg about [0001] over a distance of approximately $7\ \mu\text{m}$ on the facet. (b) High-resolution ($0.35\ \mu\text{m}$ step size) inverse pole figure map (+ image quality overlay) of the as-received material, and (c) cumulative misorientation distributions along profiles (1) and (2) in (b). (Color figure online).

compared with all of the others investigated in the current study. This was because the facet surface topography (roughness), which was the primary indicator of crack length in the continuously cycled specimen, was relatively consistent throughout the entire faceted region. Several representative propagation facets are shown in Figure 11. These facets had markings on their surfaces that corresponded well with the overall sense of crack propagation. After examining several millimeters of the faceted region at magnifications greater than 800 times, a single facet was identified at a subsurface location that had the planar, featureless surface topography characteristic typically associated with crack-initiation facets. This facet is identified as ST-1 in Figure 12. The surrounding facets were characterized as propagation facets, and those in the immediate vicinity of the initiation site were both inclined and nearly perpendicular to the loading direction. Although the test was conducted in laboratory air, it is important to note

that the facets formed at subsurface crack-initiation sites were not surface connected and were therefore propagating in high vacuum.

Regardless of spatial orientation, the propagation facet surfaces all had a similar appearance, which is shown in the lower portion of Figure 12. This surface topography is considerably different than that observed on the continuously cycled specimen and appears more ductile. The markings on the facet surfaces had a distinct directionality, which was consistent with the macroscopic crack propagation direction, although the orientation of these markings often changed substantially at grain boundaries suggesting that the crack propagation path was strongly dependent on crystallographic orientation, more so than those facets on the continuously cycled specimen. In general, the size and shape and density of these markings on the facet surfaces remained relatively constant throughout the entire faceted region. On each facet, there were typically

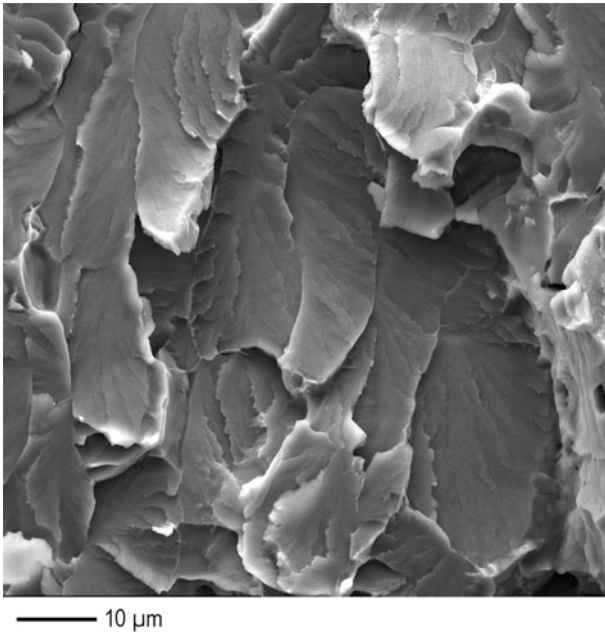


Fig. 11—Typical facet appearance throughout the entire faceted region on the specimen statically loaded in air.

several large ridges extending along the crack propagation direction. These ridges had several smaller ridges, or tributaries, branching off from them at an angle to the overall crack propagation direction. These tributaries became gradually smaller until they eventually were indistinguishable from the flat part of the facet surface between the ridges.

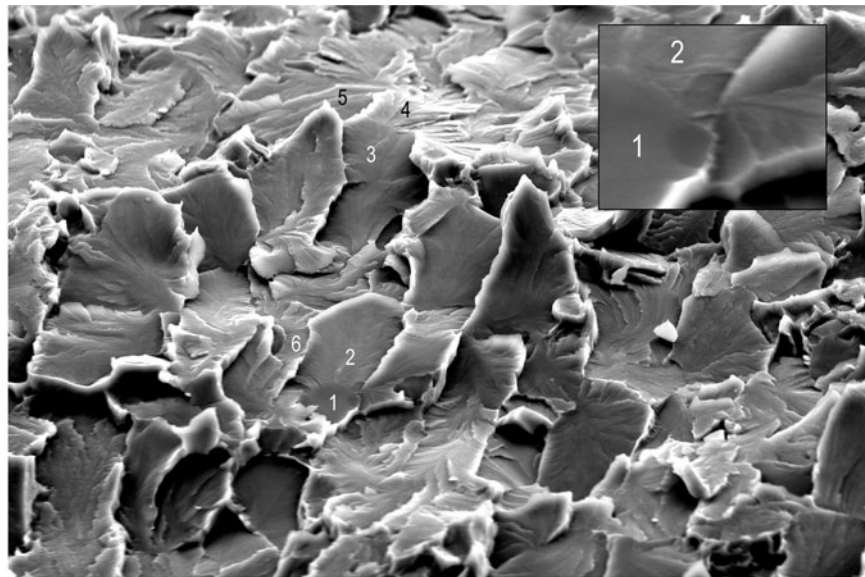
The top of the primary ridge was peak shaped and often came to a point suggesting that these features were formed by plastic flow of the α phase. Between the larger primary ridges, there was another set of shallower ridges that had similar shape termed secondary ridges. There were occasionally acicular features on the facets located near the ridges that were typically less than 100 nm long and 25 nm wide. In some locations, the features appeared as if they were particles on the facet surface, whereas in others they seemed to be partially embedded in a ridge (arrows in Figure 12). They became most apparent on the facets only when imaged with the TLD. The particles appeared bright when imaged with secondary electrons and were indistinguishable from the rest of the facet when imaged with backscattered electrons, other than contrast changes caused by variations in surface height. Although these features are often associated with ridges, their significance in the formation of the ridge markings is not entirely clear as the frequency of ridges far exceeded the density of particle-like features.

The crystallographic orientations of the initiation facet and five propagation facets (Figure 12) were studied in detail, and the results have been plotted on the inverse pole figures in Figure 13. The initiation site, facet ST-1, had a normal that was 23 deg from the loading direction while the propagation facets at the smallest crack length, ST-2 and ST-6, had angles of 18 deg and 11 deg, respectively. With regard to the

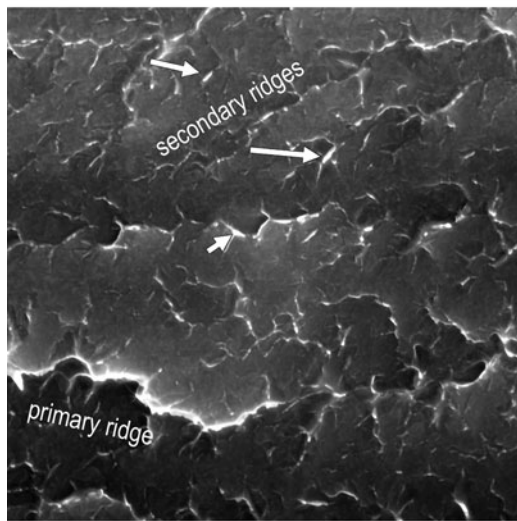
plane of fracture, ST-1 was approximately 5 deg from the basal plane, whereas ST-2 and ST-6 have fractured on planes approximately 15 deg from (0001). Similar to the case of continuous cycling, the crack initiated within a grain whose [0001] direction was inclined to the loading direction (~ 25 deg). Thus, the grain in which the crack started was oriented such that there was sufficient resolved shear stress for slip on the basal plane at the applied stress, but also a significant resolved normal stress. The nearby propagation facets were less inclined, however, than those surrounding the continuous cycling initiation facet. It is also noted that the first propagation facets, ST-2 and ST-6, were also in an orientation where they could deform easily by basal slip, both having their c axes more inclined to the loading direction than the crack initiating grain. However, despite the almost certain presence of basal slip bands, the crack clearly propagated along a crystallographic plane that was inclined to the basal plane and close to $\{10\bar{1}7\}$.

Of the facets analyzed at a slightly longer crack length (facets ST-3, ST-4, and ST-5 in Figure 12), facet ST-3 was oriented crystallographically for easy basal slip like those grains near the initiation site; however, it fractured ~ 15 deg from (0001) with a facet normal angle of 14 deg. Facet ST-3 also had two different underlying grain orientations as evidenced by the loading direction pole figure; however, when we accounted for the difference in fracture plane normal amongst the various regions on the facet where EBSD patterns were collected, the crystallographic fracture plane was similar for all data points measured. The c axes of facets ST-4 and ST-5 were oriented only 4 deg and 8 deg, respectively, from the loading direction. However, despite the high resolved normal stress on the basal plane of grain 4, it fractured on an irrational plane that was ~ 6 deg from the loading direction, whereas grain 5 had highest normal stress on the irrational plane near $\{10\bar{1}7\}$, yet it fractured precisely on the basal plane.

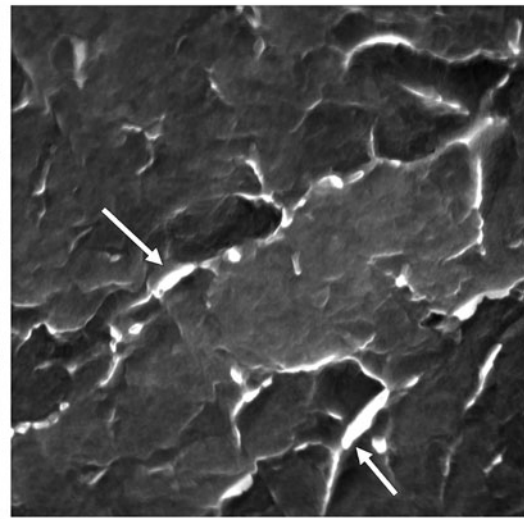
In this specimen, the initiation grain and the first few neighboring grains were in neither hard nor soft orientations. In contrast to the continuously cycled specimen, the propagation facets were less inclined to the loading direction. Under sustained loading, this might be expected because, according to fracture mechanics,^[37,38] cracks propagating in mode I have the highest strain energy release rate per unit crack advance. Thus, this would be the preferred crack propagation mode under sustained tension loading, assuming there is a crack extension mechanism available to support this. This may help explain why the crystallographic plane of fracture can be either (0001) or inclined to it. The fact that $\{10\bar{1}7\}$ occurs more frequently might be related to the fact that there are six $\{10\bar{1}7\}$ planes and only one basal plane, so it is more likely that a $\{10\bar{1}7\}$ plane will have higher resolved normal stress. The fact that the experimental data do not rigorously support this speculation (*e.g.*, facet ST-4) is likely related to crack front incompatibility and local neighborhood effects resulting in grain level stress states that are considerably more complicated than when it is assumed each grain experiences a simple “uniaxial” load, which has been shown



20 μm



500 nm



200 nm

Fig. 12—(Top) Secondary electron image of the crack-initiation site in the statically loaded specimen. Six facets are identified, which were analyzed in detail. The initiation site is shown at higher magnification in the inset. (Bottom) High-resolution images showing the facet topography of typical crack propagation facets. The macroscopic crack propagation direction is from left to right. See text for information regarding arrows.

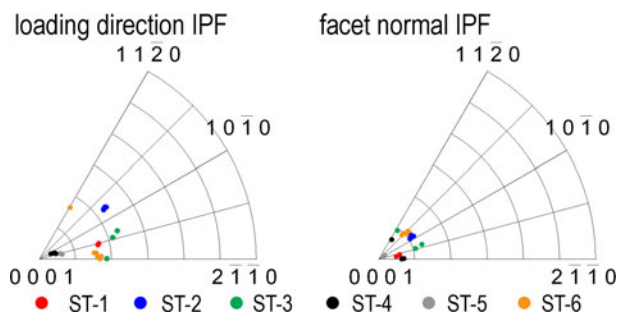


Fig. 13—Results from the facet crystallography analysis on the initiation (ST-1) and propagation (all others) facets from the statically loaded specimen. (Color figure online).

experimentally to be an invalid assumption during a tensile hold.^[39]

The EBSD analysis has shown that there was not necessarily a unique facet plane during static loading in air, although the preferred fracture plane seemed to be nearer to $\{10\bar{1}7\}$ than to (0001). Although the formation of a slip band followed by separation of the slip band because of a normal stress can describe the formation of the initiation facet, it fails to describe the formation of the subsequent propagation facets because $\{10\bar{1}7\}$ is not a slip plane, and it has essentially zero resolved shear stress. Furthermore, although the formation of faceted features is typically associated with brittle fracture, the ridges on the surfaces of the propagation facets could not have been formed without

localized plastic deformation. As will be shown subsequently, similar features were observed on the stress corrosion and dwell fatigue crack propagation facets. Therefore, discussion on the mechanism of facet formation is reserved until all data have been presented.

3. Static Loading in 3.5 Pct NaCl

The specimen that was statically loaded in 3.5 pct NaCl exhibited surface crack initiation emanating from the scribe lines; however, none of these were connected directly to any of the faceted regions. Furthermore, no faceted initiations were observed that seemed to be the result of surface slip band extrusions like those reported by Zhang and Vereecken.^[40] There was one small region of facets (Figure 14) that was within a few microns from the surface of the specimen whose features indicated that the crack was running away from the surface of the specimen. This suggests that these facets were formed at a small crack length after surface initiation in grains not suitably oriented for faceted crack propagation. Three facets from this region were analyzed in detail, labeled SCC-1, SCC-2, and SCC-3 in Figure 14. All three facets were inclined substantially to the loading direction, with facet normal angles of 31 deg, 32 deg, and 37 deg, respectively. With respect to the loading direction, the *c*-axis of the three grains was inclined between 40 deg and 47 deg to the loading direction (Figure 15). Similar to the case of static loading in air, all of the facet planes near the initiation site were coincident with an irrational {hkil} plane that was inclined to the basal plane, between 6 deg and 14 deg in this case. Slip traces were evident on some facet surfaces (SCC-2 in Figure 14, for example); however, the slip traces were not parallel to the steps or ridges on the facet surfaces that were indicative of the local growth direction.

Additional propagation facets were analyzed in a different faceted region near the surface on the opposite side of the specimen where the crack was growing toward the free surface (Figure 16(a)). Similar to the specimen statically loaded in air, these propagation

facets were typical of those observed throughout the rest of the faceted regions in this specimen. At longer crack lengths, the ridges on the facet surfaces were more similar in appearance to those in the specimen statically loaded in air except there were almost no tributaries extending from the primary ridges transverse to the primary growth direction as there were in the specimen statically loaded in air. The difference in the facet surface topography is most likely a result of the difference in environment at the crack tip. The facets in Figure 12 were formed before the crack was surface connected and therefore was propagating in a vacuum, whereas the facets in Figure 16 were formed in the presence of a mildly corrosive 3.5 pct NaCl solution. The main difference between the facets on the two specimens were the tributaries, which branched out from the primary ridges on the statically loaded specimen (Figure 12), but not the 3.5 pct NaCl solution (Figure 16). In addition, the peaks of all the ridges exposed to 3.5 pct NaCl seemed to have been “smoothed” by the electrochemical reactions that occur at open circuit potential. However, the ridges on the facets of the specimen loaded in air (Figure 12) remain in the state in which they were

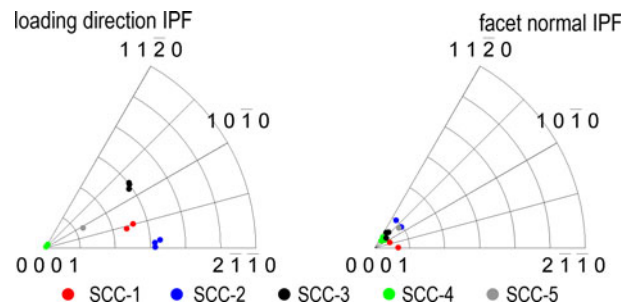


Fig. 15—Initiation and propagation facet crystallography for the as-received SCC specimen. Facets SCC-4 and SCC-5 are propagation facets, whereas the others are the near-initiation site facets. (Color figure online).

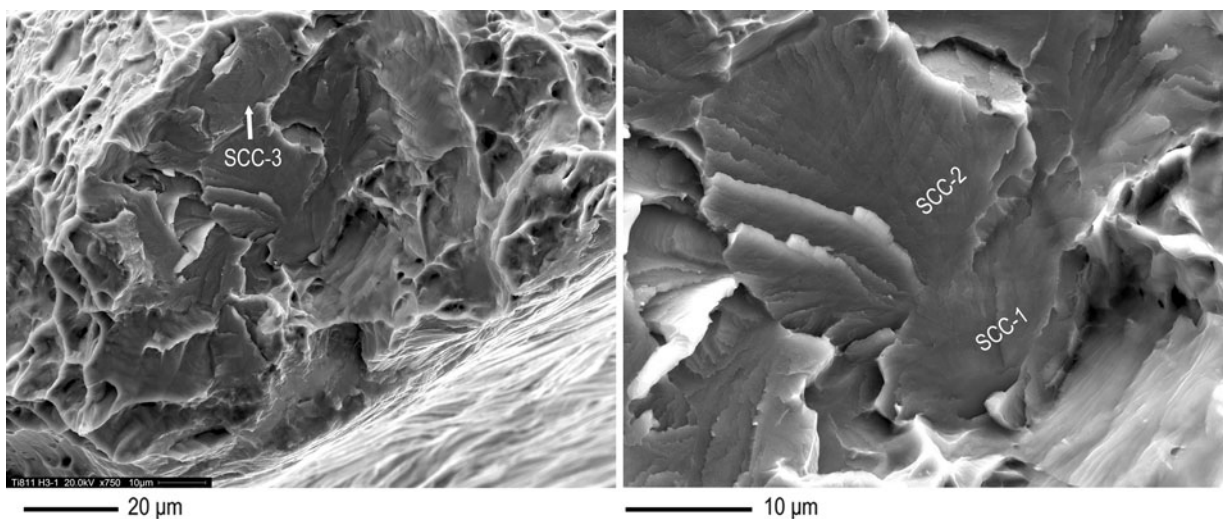


Fig. 14—The facets nearest to the surface of the sample on the specimen subjected to static loading in 3.5 pct NaCl at 95 pct of the yield strength.

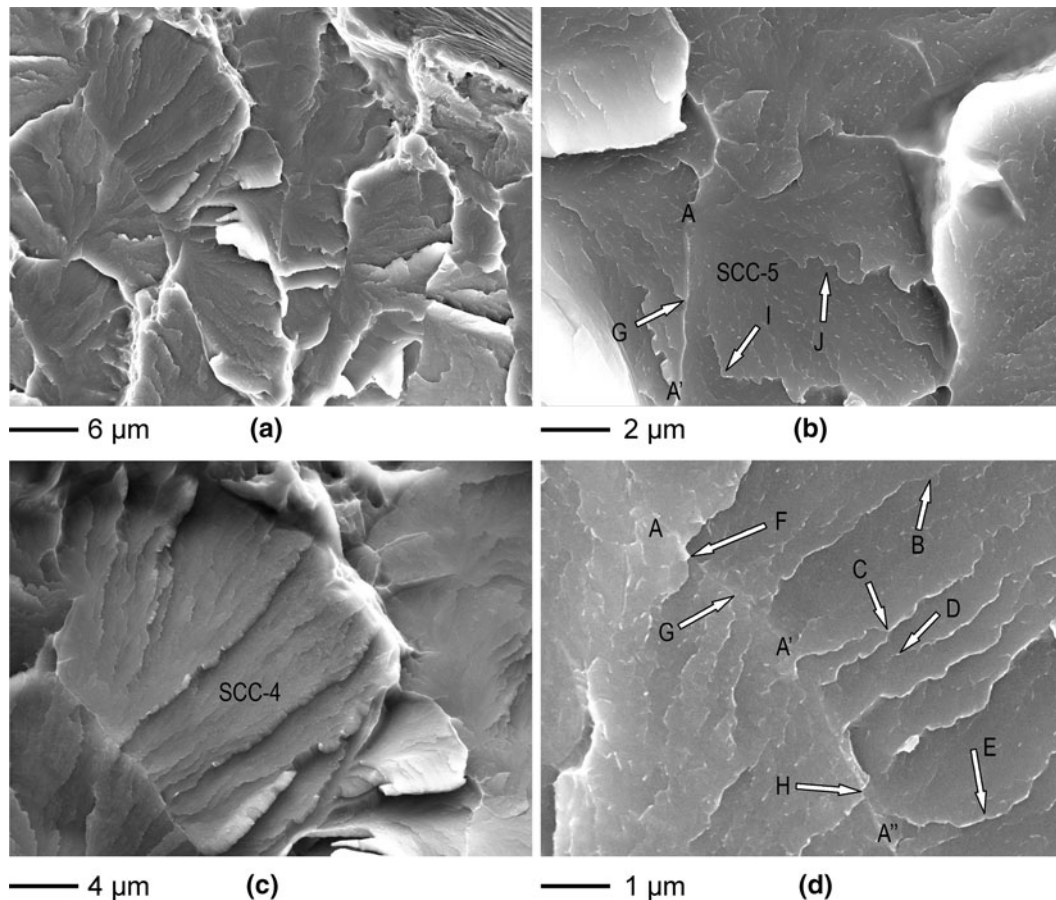


Fig. 16—Propagation facets on the fracture surface of the specimen subjected to static loading in 3.5 pct NaCl at 95 pct of the yield strength. Those facets analyzed in detail have been labeled with unique facet identification numbers. See text for details regarding the features identified by letters in (d).

formed. Examining the spatial and crystallographic orientations (Figure 15) of these propagation facets revealed that the facet normal directions were 7 deg and 9 deg from the loading direction. The [0001] axis of grain SCC-4 was parallel to the loading direction, yet it fractured on a plane approximately 5 deg from (0001). In contrast, [0001] of grain SCC-5 was ~19 deg from the loading direction with a fracture plane approximately 14 deg from (0001), or 1 deg from $\{10\bar{1}7\}$.

Between the primary ridges on the specimen tested in 3.5 pct NaCl, there were smaller ridges approximately 100 nm to 200 nm long that also tended to align in the nominal direction of crack propagation as in Figures 16(b) and 16(d), for example. Images acquired with the TLD reveal that the ridges behave in several different ways compared with the steps on continuously cycled specimens.^[4,30] These are illustrated by letters A through J in Figures 16(b) and (d), which show facets SCC-4 and SCC-5. Some ridges are observed to get smaller until they become indistinguishable from the facet surface as indicated by letter B. The ridges are observed to interact in many ways at grain boundaries, which are identified by line segments A-A' and A-A'-A''. For instance, at location A' in Figure 16(d), a new ridge is formed in the grain boundary, whereas one ridge approaching the boundary at F gives rise to one larger

ridge in the adjacent grain. However, at location G, a ridge is arrested at the grain boundary, and not even a small ridge is emitted into the adjacent grain. Although these ridges were all perpendicular to the grain boundary, location H shows that the ridges also may change orientation at the grain boundary and propagate parallel to the boundary before becoming orthogonal to the boundary and advancing into the next grain. Two ridges that form at a grain boundary can coalesce once inside the grain as shown by letter C; however, the grain boundary is not necessary to develop a ridge as indicated at letter D. In general, all the ridges exhibit some degree of undulation; however, the primary ridges go through extremely large curvature changes on some parts of the facet as indicated by letters E and J.

Although some ridges are observed to form internally on facets, it is clear that the crack propagates sequentially from grain to grain, and there is no evidence for multiple internal initiations ahead of the primary crack tip, which is characteristic of quasi-cleavage in quenched and tempered steels.^[41] The formation of such features must involve considerably more localized plasticity than when the crack propagates along a preexisting basal slip band. This behavior is entirely different from the observations made in the continuously cycled specimen where the number of steps on the facet surface increased

with each grain boundary encountered. Also, during continuous cycling, the overall facet surface roughness increased with increasing crack length because of the increase in the cyclic crack tip plastic zone size. In contrast, there was no direct correlation between facet surface topography (roughness) and crack length observed here even though the monotonic plastic zone size is larger than the cyclic one.^[38]

4. Dwell Fatigue

In addition to the primary and secondary initiation sites identified in the low magnification image of the fracture surface in Figure 5, another five subsurface secondary initiation sites were identified near the primary initiation site as shown in Figure 17. At least six other subsurface initiation sites were identified

throughout the rest of the faceted region that extended toward the other side of the specimen, although the search of the faceted region was by no means exhaustive. As mentioned previously, the crack would have been propagating in high vacuum throughout the faceted region in this specimen because of the subsurface initiation.

The primary initiation site (Figure 18) serves as a good example to demonstrate the necessary characteristics to be classified as *the* primary initiation site. The term “primary” implies that the location was where the first crack formed during testing for reasons that will become apparent below, whereas the term “secondary” only implies that the initiation event occurred after the primary one. The fractographic analysis could not discern the order of subsequent initiation events. This

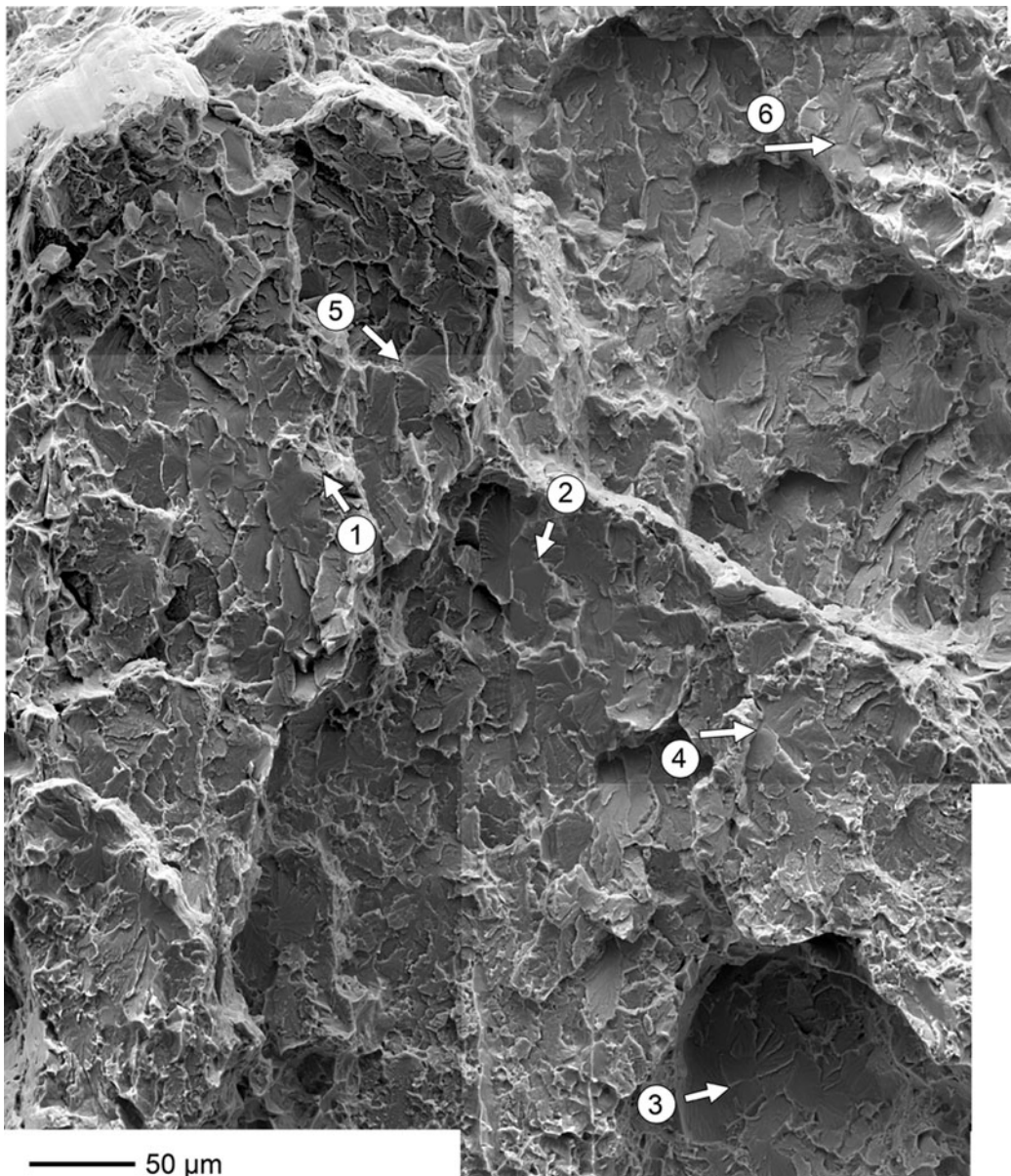


Fig. 17—Higher magnification secondary electron montage of the region around the primary initiation site (1) which reveals several secondary initiation sites (2-6).

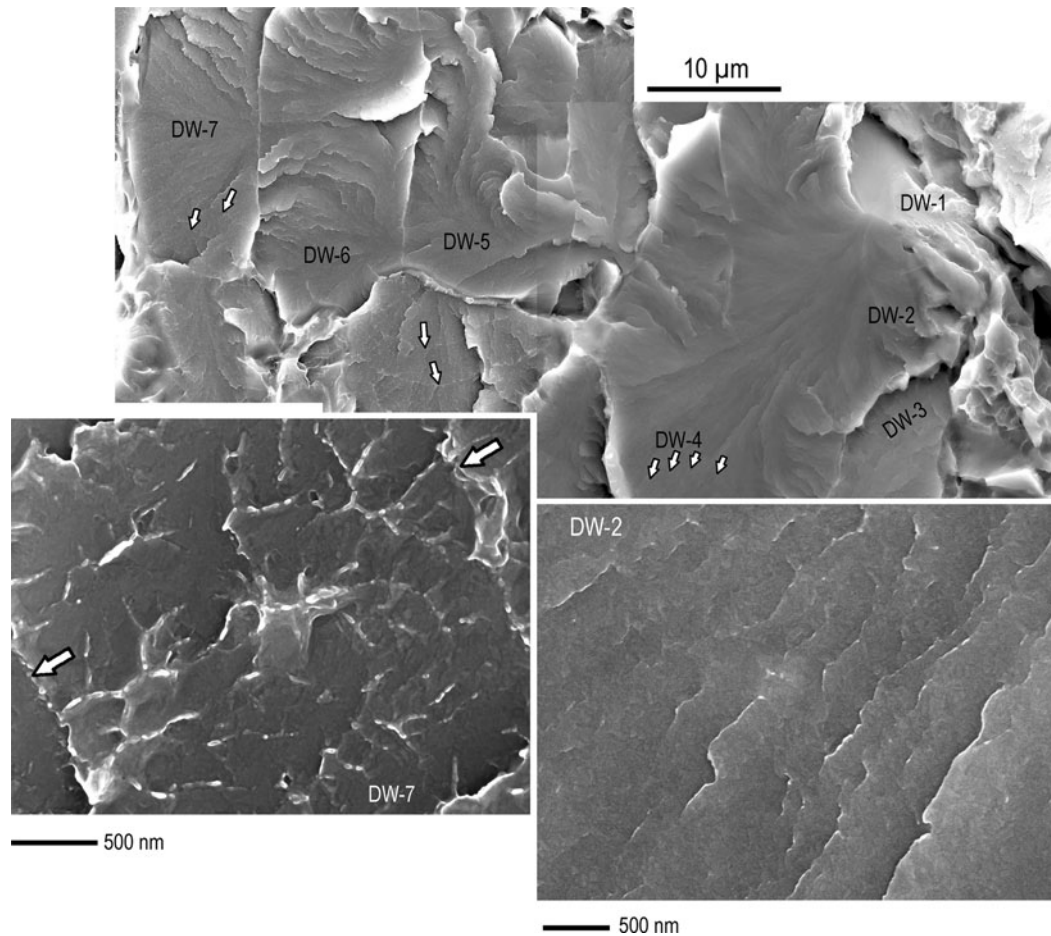


Fig. 18—High-resolution secondary electron images of the fracture surface of the dwell fatigue specimen (all at 0 deg stage tilt). The top image shows the initiation facet (DW-1), which is inclined substantially to the loading axis and subsequent propagation facets (DW-2 through DW-7). The arrows in the top image identify crack front arrest marks.

terminology is consistent with that of Uta *et al.*^[17] and also supports the authors' observation of multiple initiation events within a single microtextured region during a dwell fatigue test of IMI834. The facet topography in this region is consistent with that on the specimen statically loaded in air, with ridges extending along the direction of crack propagation. These markings lead back to the intersection two facets on the fracture surface, DW-1 and DW-2, which are shown at a higher magnification in Figure 19. There were steps on the surface of facet DW-1 and ridges on the surface of facet DW-2, both leading away from the grain boundary (segment A-A'). This implies that the crack initiated at the grain boundary where these two particular planes met. It is noted that there was extremely good mating between the facet planes over the length of the boundary, which suggests that this is a primary α /primary α boundary as opposed to a primary α /retained β /primary α or a primary α /retained β /transformed β boundary. After the crack initiated at the boundary, it propagated by faceted growth through the surrounding grains labeled DW-3 through DW-7 and beyond.

Facet DW-1 was more planar than any of the adjacent facets and had the smooth surface topography consistent with the initiation facet on the continuously

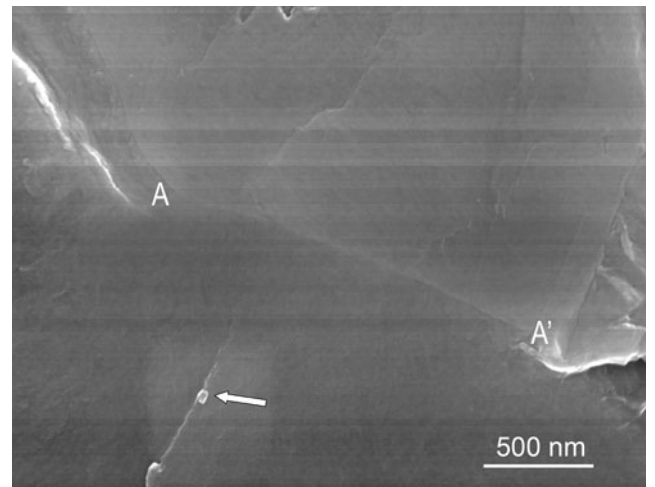


Fig. 19—The intersection of facets DW-1 (top) and DW-2 (bottom) at the primary dwell fatigue crack-initiation site. The arrow identifies a small particle near the first ridge formed on the first propagation facet. The composition and crystallographic structure of this feature is unknown.

cycled specimen. This facet normal was 41 deg from the loading direction, whereas the adjacent facet normal, DW-2, was less than 3 deg from the loading direction.

These facet planes were therefore near the maximum resolved shear stress and resolved normal stress orientation, respectively. The subsequent propagation facets, DW-3 through DW-6, were also in near-maximum resolved normal stress orientations with facet normal angles of 8 deg, 7 deg, 8 deg, and 6 deg, respectively. With regard to facet topography, facet DW-2 had a series of parallel, shallow ridges extending away from the grain boundary initiation site (Figure 18). With increasing crack length from the initiation site, these ridges became larger and began to exhibit branching, which is evident on facet DW-7. Crack front arrest marks, with spacing of 1.5 μm to 2.0 μm , were also evident on the facet surfaces at crack lengths greater than $\sim 20 \mu\text{m}$ and became more apparent at magnifications of 500 times to 1000 times at crack lengths of $\sim 100 \mu\text{m}$ (Figure 20). The primary ridges parallel to the local crack propagation direction were generally orthogonal to the crack front arrest marks. If not for these arrest marks, the dwell facets would be indistinguishable from those formed during static loading in air (but propagating in vacuum). It is noted that several arrest

marks can be observed within a single facet, indicating that these are neither cleavage nor quasi-cleavage facets, as the observed characteristics do not conform to the definition of either term as they were used originally.^[27,41] It is worth mentioning that Meyn^[42] has observed crack front arrest markings on facet surfaces of Ti-811 subjected to static loading in hydrogen gas. Considering that similar markings were not observed on either of the statically loaded specimens, we are confident that the crack front arrest markings observed on dwell fatigue facets were formed during the unload/reload cycle. The markings were also observed to change direction drastically at some grain boundaries, similar to the other loading conditions involving a static component, which suggests that this mechanism of faceted crack growth is highly crystallographic.

Surprisingly, neither the facet topography nor the crack front arrest mark spacing changed significantly with increasing crack length throughout the entire several-millimeter-long faceted region (Figure 20). At crack lengths greater than $\sim 1 \text{ mm}$ from the primary

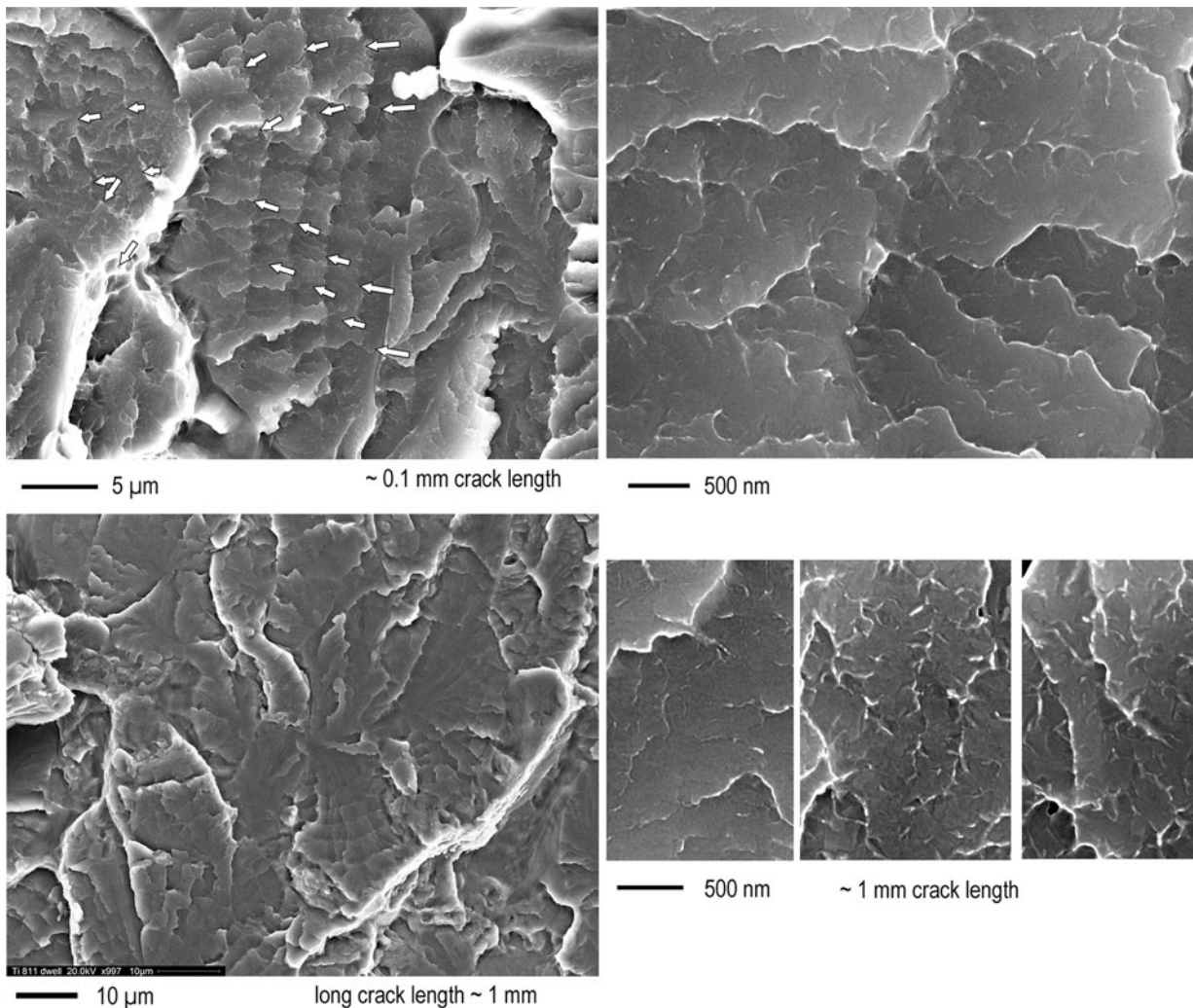


Fig. 20—Secondary electron images showing little variation among the facet surface topography as a function of crack length in the dwell fatigued specimen. A secondary initiation site is also evident in the center of the lower left image.

initiation site, the crack front arrest mark spacing was only on the order of $2.0\ \mu\text{m}$ to $3.0\ \mu\text{m}$, which is just slightly larger than that measured at crack lengths between $20\ \mu\text{m}$ and $100\ \mu\text{m}$. The facets consistently had ridges extending in the direction of local crack propagation, and there were often adjacent facets with varying areal densities of ridges. Presumably, this is an orientation dependency, although no attempt was made here to quantify it. The effect of the unload/reload cycle on the primary ridges and facet topography is evident in Figure 20. The crack front arrest markings were similar to striations in the sense that they denote the occurrence of one unload/reload cycle, but because of their curved shape marking the local crack front, they could not have formed by intersection of slip bands with the fracture surface and, thus, could not have formed by Laird's classic "sliding off" mechanism involving duplex slip ahead of the crack tip.^[43]

The crystallographic plane of fracture for the two grains involved in the crack-initiation process and several of the subsequent propagation facets was investigated using the tilt fractography/EBSD technique, and the results are reported in Figure 21. With respect to the loading direction, the *c*-axis of grain DW-1 is inclined approximately 43 deg, whereas the remaining propagation facets all have *c*-axis inclinations between 8 deg and 26 deg. After accounting for the spatial orientation of each facet, the crystallographic plane of fracture was identified as being less than 1 deg away from the basal plane for the initiation facet (DW-1) and inclined between 16 deg and 22 deg to the basal plane for the remaining propagation facets. The crystallographic misorientation angle between grains DW-1 and DW-2 was 48.6 deg, indicating that this was a high-angle grain

boundary. Furthermore, the potential for slip transfer was investigated by the method described elsewhere,^[4] and it was found that no slip systems were suitably aligned for transfer through the grain boundary. Thus, it is reasonable to conclude that this grain boundary was amenable to the formation of a dislocation pileup of significant strength.

The spatial and crystallographic orientation of facet DW-2 was measured in a different SEM to confirm the results. In addition, during this second analysis, seven EBSD patterns were collected along a line extending perpendicular to the facet boundary toward grain DW-4. These orientations are shown on the inverse pole figures in the bottom of Figure 21, which clearly reveals that the fracture plane is inclined 15 deg to the basal plane, making it near to $\{10\bar{1}7\}$. The facets on all the grains surrounding the initiation site, except DW-5, were oriented such that the *c*-axes were inclined 20 deg to 25 deg to the loading direction, indicating that they were capable of basal slip. However, all the facet normal directions were nearly parallel to the loading direction, with the largest deviation being ~ 7 deg, indicating that the fracture plane was not the basal plane but rather inclined to it, as shown in Figure 21. Other facets surrounding the primary initiation site, from which EBSD data was not collected, exhibited angles as large as 16 deg between the facet normal and the loading direction. Although these grains should have been capable of basal slip and likely developed basal slip bands during loading, they did not fracture on this plane. Instead, the fracture planes deviated between 12 deg and 23 deg from (0001), which is similar to the specimens fractured by sustained loading in air and in 3.5 pct NaCl. The similarity in spatial and crystallographic orientation and facet surface topography among the facets formed by these three types of loading suggests that all the cracks are propagating by similar mechanisms. The differences in crack growth rates and facet appearance are most likely related to the crack tip environment.

The secondary initiation site identified on the dwell specimen in Figure 5 was also examined with tilt fractography and EBSD, and the results are shown in Figure 22. The initiation facet (DW-B1) was identified by its smooth, planar surface topography, which became more apparent at large stage tilts. This facet had a normal that was 25 deg from the loading direction, whereas the two neighboring propagation facets, DW-B2 and DW-B3, made angles of 14 deg and 20 deg, respectively. After accounting for the spatial orientation, the fracture planes were determined to be between 2 deg and 5 deg from (0001) for grain DW-B1, ~ 15 deg for grain DW-B2, and ~ 16 deg for DW-B3. These observations provide additional confirmation for the initiation mechanism observed at the primary initiation site. It is argued that the primary site was more favorable for early crack initiation because of the better matching of the fracture planes in the grain boundary along with the higher resolved shear stress for slip on the basal plane of grain DW-1, allowing for easier accumulation of the necessary shear strain.

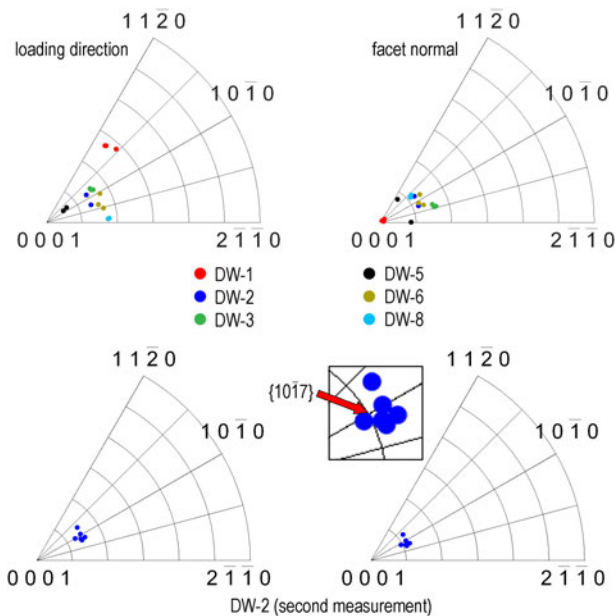


Fig. 21—Dwell fatigue facet crystallography. Equal-angle inverse pole figures showing the orientations of the faceted grains identified in Fig. 18 with respect to the loading direction and facet normal. (Color figure online).

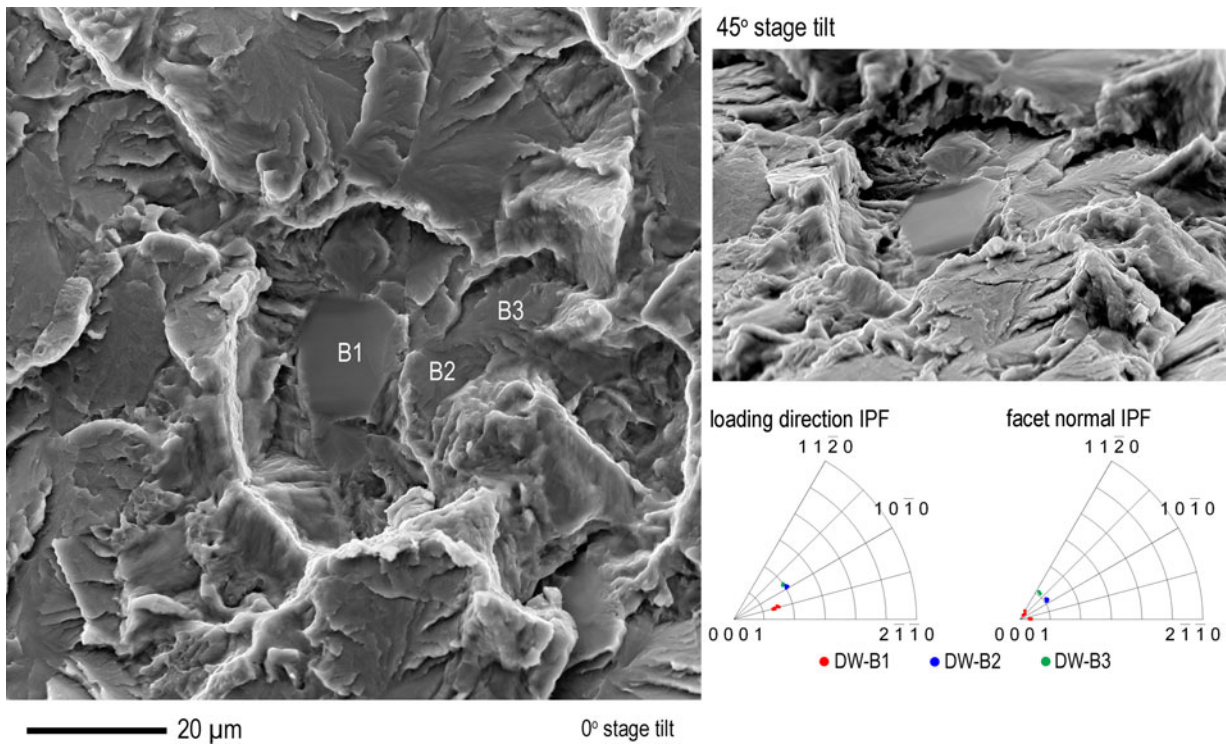


Fig. 22—Secondary electron images and facet crystallography analysis of a secondary initiation site in the dwell fatigued specimen. This location was approximately $380\ \mu\text{m}$ away from the primary initiation site. (Color figure online).

IV. FURTHER DISCUSSION: DWELL FATIGUE CRACK INITIATION AND PROPAGATION

The fractographic and crystallographic observations presented above provide further support for the reports of Sinha *et al.*^[7,8] and Uta *et al.*^[17] regarding the crystallography of dwell fatigue crack propagation facets. The authors of both investigations have reported that dwell fatigue crack propagation facets were inclined between 10 deg and 20 deg to the basal plane in the near- α alloys Ti-6242 and IMI834, respectively. Using the same technique to locate the initiation sites as we have reported here, namely, tracing the fine markings on the facet surfaces to a convergence point, Uta *et al.*^[17] identified a primary initiation site and several secondary initiation sites. The authors characterized each initiation site as containing a “pure cleavage facet with no local marks” that was surrounded by “quasi-cleavage” propagation facets. Ignoring the inconsistencies regarding the use of the words “cleavage” and “quasi-cleavage” to describe both types of facets,^[27] it is noted that crystallographically, the primary initiation site observed by Uta *et al.*^[17] is consistent with our observations. Specifically, there was one grain with its c -axis inclined to the loading direction such that it can deform by basal slip that faceted near the basal plane, resulting in a microscopically smooth, planar fracture surface. Adjacent to this was another grain whose c -axis was less inclined to the loading direction that formed a facet on an irrational plane inclined between 10 deg and 20 deg to the basal plane and that has markings indicative of crack propagation. Unfortunately, Uta *et al.*^[17] reported neither the spatial orientation of the facet

normal directions nor the facet normal inverse pole figures so no further comparison to their results can be made here. The spatial and crystallographic characteristics of the propagation facets analyzed here are, however, consistent with the measurements made on dwell fatigue propagation facets by Sinha *et al.*^[7,8]

The direct observation of several dwell fatigue crack-initiation sites (both primary and secondary initiation in the current study and by Uta *et al.*^[17] in a different alloy) that contain pairs of adjacent primary α grains similar to those described previously is potentially significant, as it seems to both confirm and contradict several things considered to be characteristic of dwell fatigue failures. First, these results confirm that indeed, a pair of grains is involved in the crack-initiation process as first proposed by Evans and Bache.^[6] Here, despite the relatively high volume fraction of transformed β , both of the grains involved in the initiation event were primary α grains. The adaptation of the Stroh model proposed by Evans and Bache^[6] contends that slip in the soft grain and the formation of a dislocation pileup is necessary to induce slip on the basal plane of the hard grain. This is necessary to obtain the necessary critical combination of shear stress (or strain) and tensile stress normal to the slip plane that is required for facet formation. This requirement for facet formation has percolated throughout the dwell fatigue literature; however, the original citation for this requirement is from the work of Wojcik *et al.*,^[2] who studied the facets formed on large, single colonies of Ti-811 subjected to continuous cycling. All but one of the single colonies studied by Wojcik *et al.*^[2] had the basal plane oriented

such that there was sufficient resolved shear stress for slip. Consequently, it would be expected that this would be the plane that accumulates damage fastest, leading to crack initiation and propagation *during cyclic loading*. The applicability of the results of Wojcik *et al.*^[2] to subsurface dwell fatigue crack initiation in a polycrystalline material is not immediately obvious. The tilt fractography/EBSD analysis presented previously showed that the crack initiated in the grain with the substantially inclined basal plane as opposed to in the “hard” grain. Moreover, the first propagation facet was actually parallel to an irrational plane near $\{10\bar{1}7\}$ that was incapable of slip. In addition, the difference in surface topography between the facets formed during continuous cycling and dwell fatigue loading are unmistakable. There is no reason in which the mechanism that forms a smooth facet directly on a basal plane that is inclined to the loading direction and the mechanism that forms a facet with ridges and rough topography that is perpendicular to the loading direction and parallel to an irrational $\{hkil\}$ plane inclined 10 deg to 15 deg to the basal plane should be the same. Thus, the requirement for slip on the basal plane of the hard grain prior to fracture is unfounded and does not seem to be necessary based on our observations.

The second point that the experimental results presented here draw into question does not relate to the adaptation of the Stroh model itself but rather how a specific orientation has been attached to the phrase “soft grain.” With the use of EBSD analysis^[44,45] and careful serial sectioning,^[28] it was observed that dwell fatigue cracks generally initiated in regions of the sample that had both hard and soft microtextured regions. The soft regions were those that were in an elastically and plastically more compliant orientation, meaning that their c -axes were nearly perpendicular to the loading direction and they could deform by prismatic $\langle a \rangle$ slip. Based on these experimental studies, the understanding of the “source slip band” in the originally proposed Stroh-like model (Figure 1) evolved into meaning a soft grain oriented for prismatic $\langle a \rangle$ slip. Several authors^[46–49] have addressed the phenomenon of room-temperature creep in the “soft grain” and the resulting stress redistribution onto the “hard grain” using crystal plasticity finite element simulations. Although there are differences among the results of the models, they generally agree on the fact that stress redistribution within the microstructure results in the formation of large stresses at, or near, the interfaces between hard and soft microtextured regions, and the spatial orientation of the interface can either increase or decrease these stresses. This latter point is useful in understanding why a crack forms at one location within the component as opposed to others with nominally the same crystallographic misorientation. However, even though the experimental observations^[28] suggest this phenomenon is occurring on a length scale consistent with the microtextured regions, some models have attempted to employ it on the grain level.^[48,50] In addition, the tilt fractography/EBSD analysis presented previously suggests that the “softer” of the two grains is one that can deform easily by basal $\langle a \rangle$ slip as opposed

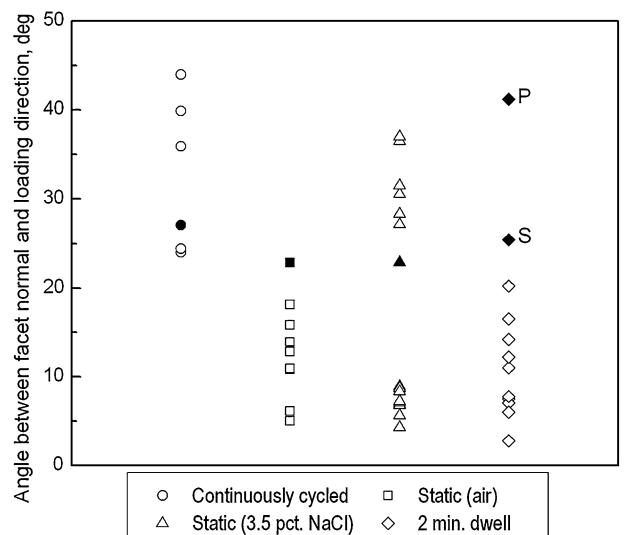


Fig. 23—Angle between facet normal and loading direction. Filled symbols indicate initiation facets, whereas open symbols designate propagation facets. Letters P and S designate the primary and secondary initiation sites studied on the dwell specimen, respectively.

to prismatic $\langle a \rangle$ slip. The “harder” grain has its c axis inclined ~ 20 deg to the loading direction, implying that it is not truly a hard grain in the sense that $\langle c + a \rangle$ pyramidal slip is not necessarily enforced, and it subsequently cracked on an irrational $\{hkil\}$ plane.

Finally, it has been reported^[6,12] that when the applied load is below the macroscopic yield strength of the material, that facets are formed nearly perpendicular to the loading direction regardless of whether a cyclic or dwell waveform is imposed. The results from the facet normal calculations as a function of loading type have been summarized in Figure 23. In this plot, the initiation facets are represented by filled symbols. It is noteworthy that initiation facets were observed on all samples with an angle around 25 deg (secondary initiation site in dwell specimen). The specimen that was statically loaded in 3.5 pct NaCl exhibited facet angles both inclined and perpendicular to the loading direction. This is most likely related to the fact that the underlying grain orientation influences fracture topography as much or more so than crack tip plasticity does. This point is evidenced by the fact that fracture topography was observed to change from ductile to faceted growth with *increasing* crack length. Furthermore, all these facets were formed below the macroscopic yield strength of the material, including those on the continuously cycled specimen, and thus the concept that facets should be normal to the loading direction^[12] does not hold rigorously.

A. Phenomenological Model for Dwell Fatigue Crack Initiation

Although the orientations of the grains at the primary initiation site of the dwell fatigue specimen have been identified, it is still necessary to describe how slip on the basal plane in the soft grain leads to crack nucleation in the boundary and subsequent faceted propagation

through the harder grains. Because of the large inclination of the initiation facets, and the presence of ridges indicative of the occurrence of plasticity on the propagation facets, neither the crack-initiation nor faceted growth mechanisms seem to be controlled by a simple normal stress criterion, *e.g.*, by “cleavage,” as some models have advocated.^[50] In this section, a phenomenological model for crack initiation and faceted propagation consistent with the experimental observations is presented. It is important to note that the dwell fatigue literature has been considered carefully while developing this mechanism; however, it may not be relevant for all alloy compositions and microstructural conditions. Recently, Brandes *et al.*^[9,51] have shown dwell sensitivity in a single-phase, equiaxed, polycrystalline Ti-7Al alloy that was thermomechanically processed *via* extrusion to have essentially no hard-oriented grains. Even in this simple material system, a significant dwell debit was observed, implying that this phenomenon is inherent in near- α (and perhaps other) titanium alloys. Whether a particular system exhibits a dwell debit in its service life would likely depend on several factors known to exacerbate the dwell effect, including but not limited to: alloy composition, microstructural condition (constituent volume fraction and morphology), interstitial content (O, H), and perhaps most importantly, the presence of microtextured regions, which provide an easy, continuous path of similarly oriented grains amenable to faceted growth.

The primary initiation site of the dwell fatigue specimen was studied extensively and even revisited on several different occasions. The spatial and fracture plane orientations presented previously were verified in two different electron microscopes to ensure consistency. It is emphasized that the fracture planes were determined from a location on the facets that did not contain any steps, and therefore, the explanation offered by Pilchak *et al.*^[27] for deviations from the basal plane caused by facet roughness does not apply here—the measured deviations from the basal plane are real. Therefore, these results are believed to be an accurate representation of the true orientations and fracture planes of the first grains to fracture during a dwell fatigue test. The discussion of the crack-initiation process will be limited to only these two grains; however, the reader is reminded that these grains are believed to exist within some volume of stressed material near the interface of a hard and soft microtextured region, which would be consistent with previous experimental observations^[8,17,44] that would place them in a region of locally higher stress caused by load shedding.

Consider the pair of grains in Figure 1 and assume the hard grain is one that is oriented with its *c*-axis approximately 20 deg from the loading direction, whereas the neighboring soft grain is oriented for easy basal slip. After the application of a load, the soft grain deforms by basal slip. Because there are no closely aligned slip systems in the hard and soft grains, the grain boundary serves as a barrier to dislocation motion, and a dislocation pileup is formed. During subsequent cycles, strain is accumulated in the basal slip band intensifying the stress concentration at the head of the

pileup. The stress concentration induces normal and shear stresses onto the planes in the adjacent hard grain. However, Koehler^[52] has pointed out that a substantial hydrostatic tension field is also created around the pileup that extends over an appreciable volume of material around the pileup. In titanium alloys, it has also been demonstrated that interstitial hydrogen is readily mobile at room temperature and that it will diffuse to regions of high hydrostatic tension, such as a stress concentration or a crack tip.^[53] Because of its incredibly low solubility in the hexagonal α phase, locally elevated concentrations of H can lead to the precipitation of a titanium hydride (even when the overall H content is low, as in the present alloy), which is a compound, often nonstoichiometric, based around TiH_x , where *x* is between 1.5 and 2. The lattice parameter and crystal structure of the hydride depends on the stoichiometry of the hydride being face centered cubic when *x* is between 1.5 and 1.8 and face centered tetragonal when it is above approximately 1.8.^[54] As mentioned by Williams,^[55] the formation of TiH_2 is accompanied by an ~18 pct change in volume, which significantly strains the surrounding matrix. In strain-free metals, the transformation strain is so large that hydride formation requires the creation of prismatic $\langle a \rangle$ dislocation loops. However, Boyd^[56] showed that slip bands can serve as effective nucleation sites for hydrides by acting as interface dislocations and reducing the elastic misfit.

With regard to dwell fatigue, there are several possible ways in which hydrogen can influence the crack-initiation process. The first possibility is that the hydrostatic stress field around the head of the dislocation pileup in the soft grain attracts hydrogen, which leads to hydride precipitation. After precipitation, a crack could form either by fracture of the hydride followed by subsequent growth into the surrounding matrix, or localized plastic deformation at the particle/matrix interface could lead to void formation and subsequent crack extension. Another possibility is that which was suggested by Troiano,^[57] where hydrogen diffuses to regions of high triaxial stress and lattice defects, which promotes microcrack nucleation after reaching a critical concentration level. Hack and Leverant^[5] have attempted to use this mechanism to explain dwell fatigue crack initiation in fully lamellar near- α alloys, but they suggested that propagation occurs by the repeated formation and cracking of hydrides at the crack tip. No convincing evidence was provided for either mechanism. The third and most attractive based on the current experimental results is that of hydrogen enhanced localized plasticity (HELP).^[53] As summarized by Robertson and Birnbaum,^[58] over a period of approximately 20 years, there have been repeated direct observations in the TEM that hydrogen influences the mobility of edge, screw, partial, and grain boundary dislocations in ordered and disordered face-centered cubic, body-centered cubic, and hexagonal close-packed materials. This accelerated dislocation behavior under constant applied stress was observed in all metallic systems in which hydride precipitation would be expected and is observed. Of particular interest is their

work on near- α titanium alloys in which Shih *et al.*^[53] showed this behavior caused a localized softening effect in the α phase of Ti-4Al. Under positive pressure of H₂ gas, hydride precipitation, growth, and subsequent fracture by cleavage of the hydride was observed. However, when observing dynamically growing cracks that were propagating too fast for hydride precipitation, a change in fracture mechanism from brittle hydride cleavage to localized ductile fracture was observed. In this mechanism, the dislocation enhancing H atmosphere resulted in slip localization, highly constrained plasticity, and extremely localized fracture at regions of highest H concentration. On a fracture surface, this type of failure is manifested as tear ridges and dimples,^[58] both of which were observed on the facets in the dwell and static-loaded specimens.

The HELP mechanism is clearly the most consistent with the experimental observations made on the propagation facets in the current study, as it can help explain the localized formation of tear ridges on the facet surfaces. The occurrence of localized softening and slip resulting from the hydrogen atmospheres is believed to accommodate the plastic strain required to locally form an instability on the facet surface, which is similar to a “neck” in a tensile test, leaving a ridge as the crack advances during the hold period. Subsequent support for the role of hydrogen in dwell fatigue crack propagation can be found in the results of the spatial and crystallographic orientation analysis. Crack propagation from the first grain occurred on planes nominally perpendicular to the loading direction that were coincident with irrational $\{hkil\}$ planes inclined between 10 deg and 15 deg to the basal plane as opposed to on (0001), as was observed during continuous cycling.

Reviewing the spatial and crystallographic orientations of the grains at the dwell fatigue crack-initiation site (Figure 21) reveals that the harder grain, the first propagation facet, has a $\{10\bar{1}7\}$ plane oriented within ~ 2 deg of the applied loading direction (maximum mode I component). Similar occurrences can be found in the surrounding dwell propagation facets as well as in the specimens statically loaded in air and in 3.5 pct NaCl, which, along with their similar surface topography, suggests that these facets all formed by a similar mechanism. We have already discussed why a facet in this spatial orientation would be preferred from a continuum mechanics perspective because of its high energy release rate; however, it has yet to be explained mechanistically why fracture occurs preferentially on irrational $\{hkil\}$ plane as opposed to low index planes. This is a particularly intriguing problem considering that many basal planes are inclined sufficiently to the loading direction so that it can be argued that they have dislocations present that, presumably, lower the cohesive strength of that plane from a defect-free crystal.

Several hydride habit planes have been reported in titanium alloys depending on alloy composition^[55] and hydrogen content,^[59] among other factors, including (0001), $\{10\bar{1}0\}$, $\{10\bar{1}2\}$, $\{10\bar{1}4\}$, $\{10\bar{1}7\}$, and $\{10\bar{1}\bar{7}\}$. Of particular interest are the basal planes and those habit planes that are only slightly inclined to it, like $\{10\bar{1}7\}$ and $\{10\bar{1}4\}$, which are approximately 15 deg

and 24 deg from (0001), respectively. These habit planes are inclined approximately the same amount from (0001) as most of the fracture planes observed on the dwell and statically loaded specimens. However, the habit planes mentioned previously were determined primarily in binary experimental alloys created by the float zone electron beam method, charged with H in a Sieverts apparatus, and then heat treated and slowly cooled to produce large hydrides observable by optical microscopy. The presence of applied or residual stresses, however, can significantly affect the precipitation process,^[55,59-61] resulting in a change in the orientation of the preferred habit plane. In fact, the effect of elastic stresses on hydride precipitation and the habit plane orientation has been recognized since the early 1960s.^[62,63] Under a tensile load, the preferred habit plane is the one that is closest to perpendicular to the loading direction because it accommodates a portion of the large strain necessary for hydride nucleation. Perhaps only by coincidence, this is also the approximate orientation of the faceted fracture planes. It is worth mentioning that similar phenomena have been observed experimentally^[64] and addressed theoretically^[61,65] for zirconium hydrides. In fact, it is generally accepted that stress-dependent hydride precipitation followed by subsequent fracture of the hydrides is the primary cause of early fracture of zirconium alloys used as structural components in nuclear reactors.^[64]

The coincidence of the crystallographic fracture plane with a hydride habit plane known to form under the influence of an externally applied stress provides circumstantial evidence that hydride precipitation may be involved; however, there is currently no direct evidence of this available on the fracture surfaces. Thus, it is useful to understand the facet surface topography associated with formation and/or fracture of a hydride particle. Consider the fractographs from the study by Yeh and Huang^[66] that have been reproduced in Figures 24(a) and (b). These facets were formed in Ti-6Al-4V by static loading a compact tension specimen in H₂ gas of varying pressure at a variety of temperatures. The similarity between these facet surfaces and those on the Ti-811 specimens subjected to dwell and static loading investigated here are unmistakable. The facets contain ridges of varying height extending in the direction of crack propagation with smaller tributaries branching off from them. There were disk-shaped features on the surface of the facet formed in 505 kPa H₂ gas at 368 K (95 °C) but not on the facet formed in 101 kPa H₂ gas at room temperature. On the former facet, one of the larger disk-shaped precipitates seems fractured, and there is evidence of void growth around the particle as it is sitting in a shallow dimple. Similar features were not observed on the latter facet (101 kPa; 293 K or 20 °C), which instead had fine acicular particles sitting on the facet surface that were often associated with the ridges. Rusli^[67] has described similar features on the facet surfaces of a Ti-8Al-1Mo-2V alloy fractured in ~ 10 kPa H₂ gas at a constant displacement rate of 0.5 mm min⁻¹ after fatigue precracking. Rusli^[67] has captured some of the particles in an acetate replica of the fracture surface and observed them directly in the

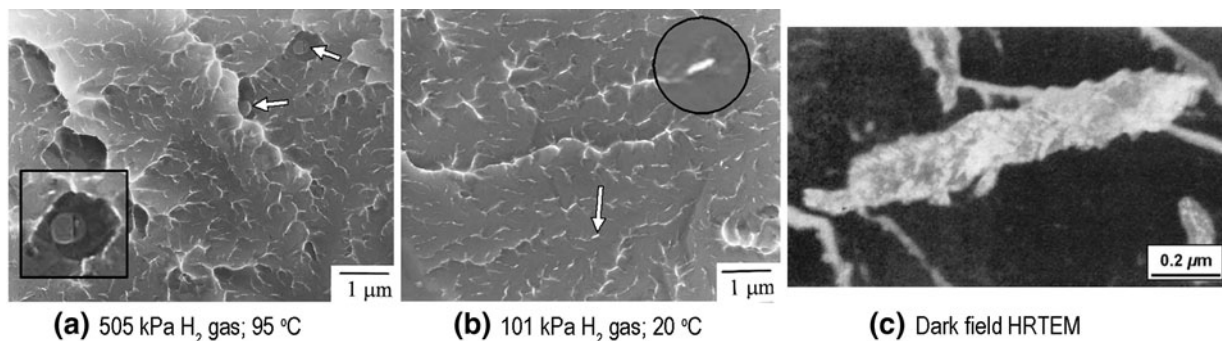


Fig. 24—(a) and (b) Surface topography of facets formed by static loading in Ti-6Al-4V alloy in H₂ gas.^[66] The arrows in (a) point to features that are presumably plate-like TiH₂ precipitates, the top of which is shown at higher magnification in the 1- μ m-wide inset. Smaller, bright particles similar to those observed on the Ti-811 facets in the current study were also observed. One is identified by the arrow in (b) and also shown at higher magnification in the 0.5- μ m diameter inset. (c) A dark field TEM image of a precipitate like the one identified in (b), except in the alloy Ti-8Al-1Mo-2V, lifted from the fracture surface in an acetate replica.^[67]

TEM (Figure 24(c)). Based on selected area electron diffraction analysis, he reported that these particles were indeed hydrides that precipitated in the α phase. None of the smaller particles were observed to be fractured like the larger, disk-shaped particles observed by Yeh and Huang.^[66]

The finer, acicular shaped particles observed on the facets in Yeh and Huang's study^[66] and also by Rusli^[67] were similar in size and morphology to features observed on the propagation facets of the dwell fatigue and statically loaded specimens. An example from the former is shown in Figure 25; however, it is noted that neither the chemistry nor crystal structure of this feature are known. Attempts to capture these particles in acetate replicas were made in the current study; however, none were found when observed in the TEM, suggesting that they were either rigidly adherent to the facet surface or that they were simply fractured titanium that seemed brighter in the TLD and were not actually a different constituent. Robertson and Birnbaum^[58] have argued that no single hydrogen-related mechanism can explain all experimental observations, and it is likely that more than one operates in a given specimen. Thus, it is enticing to conclude that the HELP mechanism seems to dominate facet formation, although those hydride variants with habit planes perpendicular to the stress axis could precipitate and assist in the fracture process by promoting formation nearly parallel to their habit plane (and perpendicular to the loading direction). Because there is no evidence of fractured hydrides on any of the facet surfaces on the specimens studied here, it is likely that hydrides (if present) exert their influence through localized deformation at the particle/matrix interface. This type of deformation behavior can rationalize both ridge formation as well as the coincidence between the fracture plane and hydride habit plane. Because there was no hydrogen gas at the crack tip of any of the specimens in the current study, it is necessary to invoke the (relatively low) internal hydrogen content of the alloy as the source of hydrogen to account for the observed features in the dwell fatigue and creep specimens. Clearly, hydrogen was available abundantly in the SCC experiment, which is the exception and might help

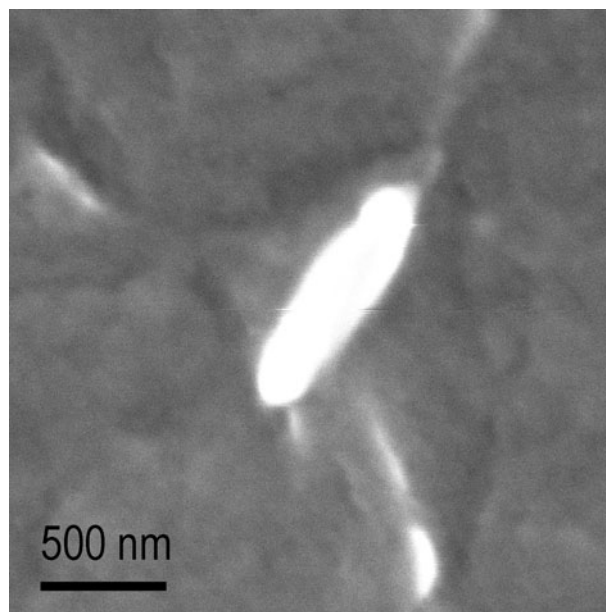


Fig. 25—Secondary electron image (TLD detector, magnification of 256,000 times) of a possible hydride particle from a dwell fatigue propagation facet.

explain the considerably faster failure times of these samples. As mentioned previously, the frequency of the potential hydride particles on the facets was considerably lower than that of the ridges, and so it is believed that the formation of these is not essential for ridge formation. It is possible, however, that after fracture, the dilatational stress field is relaxed, liberating hydrogen that can diffuse back to the crack tip, and the process repeats. This last point is difficult, if not impossible to prove for bulk specimens, and to our knowledge there have been no observations of this in thin foil studies either, but the minimal constraint in thin foils could preclude this effect anyway.

Additional support that hydrogen may play a role in dwell fatigue crack propagation process is contained within the crack growth rates as inferred from the features on the facet surfaces. The spacing of the crack

front arrest markings was determined by projecting vectors into the plane of fracture using the quantitative tilt fractography method. The magnitude of the vectors could be related to a physical dimension through the known working distance, SEM magnification, and image resolution. This ensures that the spacing measurements are not subjected to uncertainties associated with those made on two-dimensional images in which the feature of interest is inclined to the viewing direction. Near the initiation site and within the first several hundred microns, the arrest mark spacing was on the order of $1\ \mu\text{m}$ to $1.5\ \mu\text{m}$ per cycle, whereas at longer crack lengths $>1.5\ \text{mm}$ and throughout the entire faceted region, the crack front arrest marks saturated to a value between $2.0\ \mu\text{m}$ and $3.0\ \mu\text{m}$ per cycle. As a comparison, recall that the crack was advancing at a rate of approximately $150\ \text{nm cycle}^{-1}$ (Figure 8) at a crack length of $\sim 100\ \mu\text{m}$ in the continuously cycled specimen. From this value, the crack front indicators on the continuously cycled specimen gradually increased with increasing crack length, eventually evolving into classic fatigue striations. If the internal lattice resistance were the only force responsible for retarding crack growth during dwell fatigue, then the crack growth rate should increase monotonically with increasing crack length because the cyclic crack tip plastic zone has a square dependence on ΔK similar to the continuously cycled specimen. This observation is potentially important, especially when considered in the context of two other relevant facts. First, the size and shape of the faceted region reflects the underlying microtextured bands that were observed in the as-received material, and second, the apparent facet surface roughness of the dwell propagation facets does not increase systematically with increasing crack length. Both observations suggest that the fracture process is not controlled solely

by the size of the crack tip plastic zone, but rather it is a time-dependent growth mechanism. The fact that the size and shape of the faceted regions is similar to those of the microtextured regions in all of the specimens subjected to a sustained mode I loading condition implies that the crack grew preferentially through this region before extending into the surrounding microstructure. This assertion is supported by results from nondestructive evaluation measurements performed on an additional sample from this study, which did not fail after 26,263 dwell cycles. A subsurface crack was identified in the gauge section of the specimen after reconstructing the entire volume with x-ray computed tomography (Figure 26). These data, which are shown from two orthogonal directions, reveal an internal flaw that is approximately 2.4 mm long, 0.25 mm wide and is oriented perpendicular to the loading direction. The size and shape of this flaw is entirely consistent with the size and shape of the microtextured regions observed in the as-received material as well as within the faceted regions on the other specimens. This observation has important implications on variability of dwell fatigue life in laboratory specimens. For instance, the faceted region on the dwell specimen studied in detail here intersected the surface of the specimen, resulting in a larger stress concentration and exposure of the laboratory environment to the crack tip, both of which can accelerate crack growth rates through the nonfaceted regions. In contrast, the specimen shown in Figure 26 had already experienced more than double the number of cycles and revealed no significant crack growth into the adjacent microstructure. This sample failed after an additional 2,604 dwell cycles after the image in Figure 26 was taken.

Under continuous cycling, crack growth rates are slower when the nominal fracture plane is parallel to the

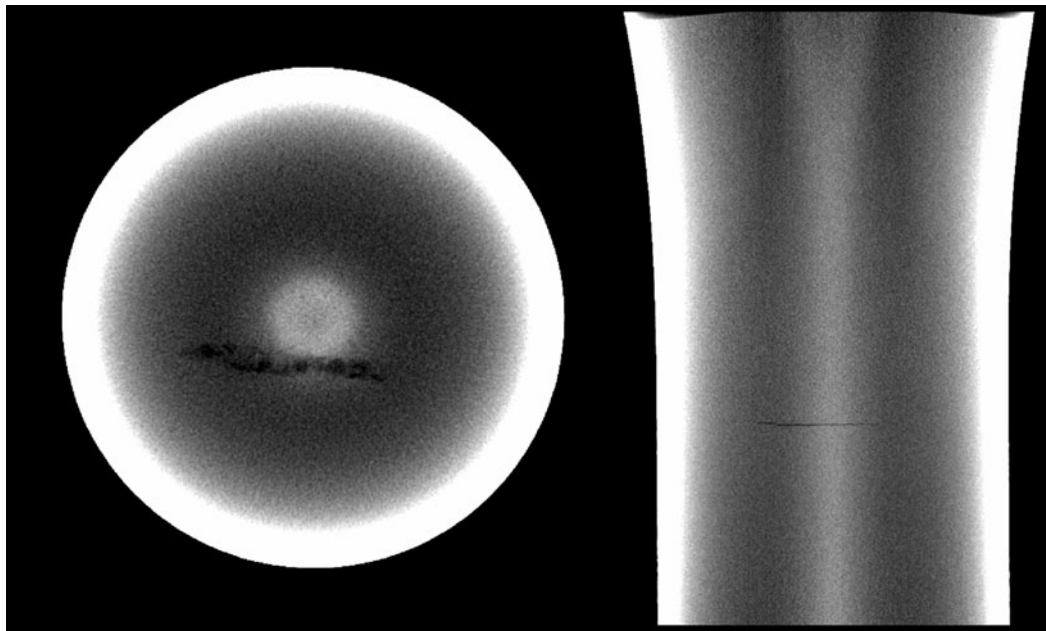


Fig. 26—Two orthogonal views of a subsurface crack imaged with X-ray computed tomography in a dwell specimen that had not failed after 26,263 cycles.

basal plane and is also perpendicular to the loading direction, *i.e.*, there is no shear stress on the basal plane. This has been demonstrated for strongly textured Ti-6Al-4V by Bowen^[68] as well as for single colonies of Ti-811 by Wojcik *et al.*^[2] Presumably, this is because of the higher critical resolved shear stress required for $\langle c + a \rangle$ dislocations to glide, which would be required to permit crack tip opening to occur plastically as in Laird's classic mechanism for fatigue striation formation.^[43] However, orientation dependencies and texture effects during dwell fatigue crack growth (and other waveforms that involve a sustained load) are arguably less well understood. As mentioned by Brandes,^[9] there are contradicting reports in the literature on the effect of dwell periods on fatigue crack propagation rates.^[15,26,69–74] Some researchers find increased crack growth rates, whereas others measure no difference, and some even find reduced growth rates. The relevance of these studies has been called into question,^[9] however, because they generally focused on long cracks growing in air as opposed to internally initiated cracks that are not surface connected, which are growing in a vacuum. The markings on the dwell and continuously cycled specimens that indicate the position of the crack front on successive cycles have shown that crack growth rates are several orders of magnitude faster in the faceted region for the dwell fatigue specimen compared with the continuously cycled one for the same crack length. In addition, having established that the size and shape of the faceted region is dictated by the underlying microtextured regions and that the crack forms within and propagates preferentially through these regions, it becomes clear that the crack growth rates outside of

the faceted region during dwell fatigue are even less important to the total life. The fact that crack growth rates measured on compact tension specimens are often insensitive and occasionally slower during dwell loading further suggests that the crack initiation and small crack growth stage are more critical to explaining the observed life debit. The reduction in the number of cycles to crack initiation resulting from dwell loading is obvious; however, the considerably higher growth rates measured directly from the facet surfaces in the current study suggest that the faceted crack growth stage is equally or even more important. This concept is consistent with the recent work of Toubal *et al.*,^[75] who have suggested that specimens with better resistance to crack propagation exhibit longer dwell fatigue lives, although the authors have not identified the particular importance of resistance to faceted growth.

Now that the preferred orientation of crack initiating grains and crack propagation grains has been identified, it is possible to discuss the effect of microtexture region size on dwell fatigue life. Consider the EBSD map of the entire transverse cross section of the dwell fatigue specimen gauge section collected approximately 1.3 mm below the fracture surface but within the reduced section of the specimen (Figure 27). These data illustrate that there is a range of sizes and aspect ratios of microtextured regions with c -axes near, or slightly inclined to, the loading direction (red hues), and so it becomes useful to understand why crack initiation might be favorable in one location compared with another. In addition, once a crack has initiated, it is useful to know which neighborhoods will facilitate faceted crack growth and ultimately lead to fracture of the component in

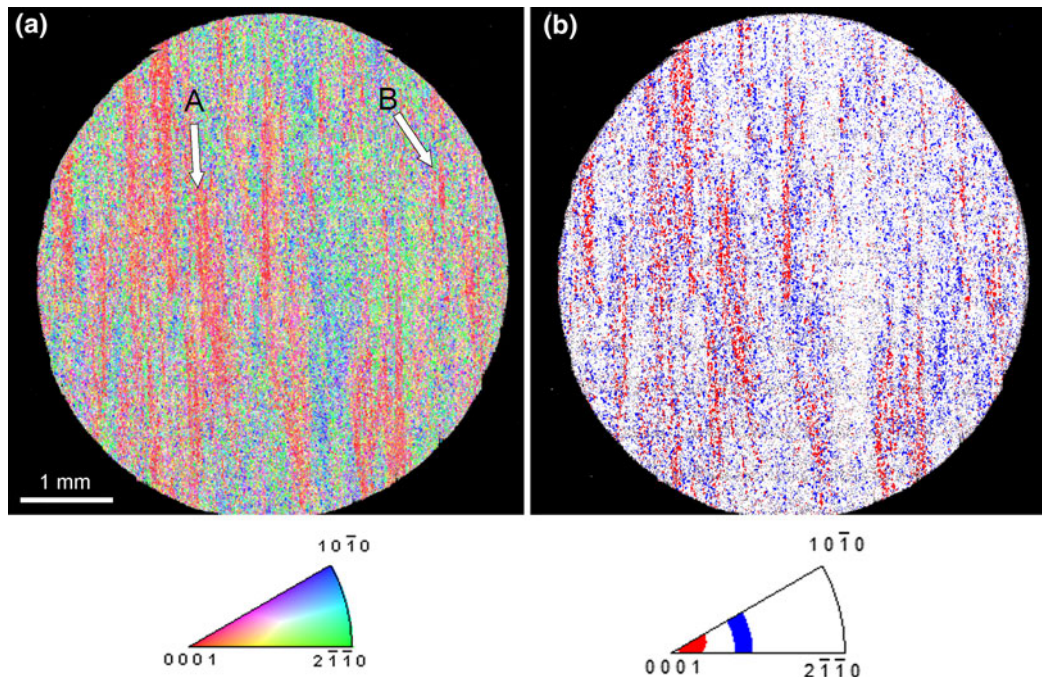


Fig. 27—(a) Loading direction inverse pole figure map of a transverse cross section of the dwell fatigue specimen approximately 1.3 mm beneath the fracture surface. In (b), those grains with basal poles inclined 40 deg to 50 deg from the loading direction have been colored blue, whereas the red grains are those with a $\{10\bar{1}7\}$ plane that is no more than 10 deg away from being orthogonal to the loading direction, as indicated by the inverse pole figures beneath each diagram. See text for details regarding locations A and B in (a). (Color figure online).

comparison with those that result in crack arrest. For discussion purposes, consider the following simple example.

Two cracks initiate on the same dwell cycle at locations A and B in Figure 27(a). They initiate at grains like those described in detail above that happen to be near the interface between “hard” and “soft” microtextured regions because of the locally higher stresses developed here because of load shedding.^[46] After crack initiation, continued growth of the crack depends on its surrounding microstructure. Based on the tilt fractography/EBSD studies, we have identified that grains with $\{10\bar{1}7\}$ planes nearly perpendicular to the loading direction provide easy propagation paths. Thus, in Figure 27(b), we have color-coded grains with high resolved shear stress on the basal plane, initiation grains, in blue, whereas the easy propagation paths are identified by the color red. Both cracks advance on each subsequent dwell cycle through their respective microtextured regions. After reaching the edge of the microtextured region, crack B is arrested because the soft-oriented grains on the other side can accommodate its plastic zone, similar to what has been observed during continuous cycling.^[30,76] The crack does not grow readily because there are no more basal planes suitably oriented for faceted growth. Crack A, on the other hand, continues to propagate through the larger microtextured region until it reaches a soft-oriented grain. Outside the faceted region, dwell fatigue cracks have been observed to propagate by more conventional striation growth,^[26] which is controlled by crack tip plasticity. Therefore, it is reasonable that the driving force for subsequent crack propagation is proportional to ΔK , which would be considerably larger for crack A, suggesting that it would most likely propagate to catastrophic failure as has been suggested by Sinha *et al.*^[28] Thus, the size and shape of the microtextured region is the most important attribute affecting dwell fatigue life because, in materials with large microtextured regions, a large internal crack can develop while the crack is still growing at high rates under relatively microstructure insensitive conditions until faceted growth is exhausted. Then, this internal flaw serves as the initial condition for the second stage of crack growth, which seems to occur by more conventional striation growth mechanisms. For modeling purposes, it is likely that the size and morphology of the microtextured region could be used to select an appropriate K solution to model subsequent plasticity controlled long crack growth.

V. OUTLOOK AND FUTURE EFFORTS

Previously proposed dwell mechanisms based on hydrogen have been criticized in the past because of their inability to explain the relatively large strain accumulation associated with dwell fatigue. Measurements of bulk strain accumulation, however, include contributions from all of the grains within the sample that, because of recent experimental and modeling efforts, are known to be plastically deforming at room

temperature. Thus, it would certainly be possible to have substantial strain accumulation at the component level while simultaneously forming and propagating a large internal crack by a process involving extremely localized plasticity, such as that afforded by the HELP mechanism.

Based on the experimental results presented here, and after careful, collective consideration of the relevant literature, we propose that the question regarding the role of hydrogen during dwell fatigue be revisited. Because of the large number of factors that influence dwell fatigue susceptibility and their apparently synergistic interactions, future experiments need to be carefully designed to probe a specific effect while maintaining the other factors constant. Experiments conducted in our laboratory^[77] have shown an increase in dwell fatigue life with increasing hydrogen content. However, a reexamination of the fracture surfaces in light of the current results revealed that the size of the faceted region varied from sample to sample. It was observed that dwell fatigue life increased with decreasing faceted region size. Perhaps only by chance, the relative size of these regions scaled inversely with hydrogen content. Because the hydrogen charging temperatures were too low to induce changes in microstructure or texture, this implies that the effect of microtexture region size overshadows the effect of hydrogen, at least for bulk concentrations up to 230 ppm, which exceeds specification limits. This finding demonstrates the need to study simple material systems in which one variable can be changed at a time to gain a more thorough understanding of all the individual mechanisms associated with dwell fatigue crack initiation and propagation. Only by understanding the individual contribution of each variable (such as microtexture region size, hydrogen content, texture, primary α volume fraction, environment) will it be possible to begin to understand the interrelations among them.

VI. CONCLUSIONS

The facets formed under cyclic, static (in air and 3.5 pct NaCl), and dwell fatigue loading were characterized with quantitative tilt fractography, EBSD, and ultra-high-resolution SEM. All the facets formed with a tensile hold component (static and dwell) exhibited similar spatial, crystallographic, and topographical features. In particular, these facets were oriented for near-maximum mode I loading and were observed to be *consistently* inclined to the basal plane. More specifically, the following conclusions were reached regarding crack initiation and faceted crack growth that occurs under different loading conditions.

A. Continuous Cycling

- Fatigue crack initiation occurred at the surface of the specimen in a grain whose basal pole was inclined 25 deg to the loading direction.
- Subsequent propagation also occurred on basal planes that were inclined between ~ 22 deg and

41 deg to the loading direction, although some facets with unique surface topography were found to be $\{10\bar{1}0\}$ fracture planes.

- Markings on the facet surfaces that resemble fatigue striations indicated that the crack growth rate was on the order of $150 \text{ nm cycle}^{-1}$ at crack lengths as small as $100 \mu\text{m}$.
- Facet surface roughness and crack growth rate increased with increasing crack length consistent with plasticity controlled crack propagation.

B. Static Loading in Air

- Subsurface crack initiation occurred on a facet inclined ~ 23 deg to the loading direction producing a smooth facet nearly parallel to the basal plane.
- Subsequent crack propagation occurred on irrational $\{hkil\}$ planes inclined between 7 deg and 20 deg to (0001). Around the initiation grain, the propagation facets were more inclined to the loading direction than at longer crack lengths. Several crystallographic fracture planes were consistent with known hydride habit planes, although no direct evidence of hydrides were found.
- The facet surface topography was consistent with that formed by cracking in small positive pressures of hydrogen gas consisting of tear ridges extending in the direction of crack propagation.

C. Static Loading in 3.5 Pct NaCl

- Although no surface initiation facets were identified, it was evident that the preferred crack propagation plane favored being perpendicular to the loading direction regardless of the precise $\{hkil\}$ plane of fracture.
- Of the facet planes analyzed, all were inclined between 5 deg and 15 deg to the basal plane in their respective grains.
- The facet surface topography consisted of ridges extending in the direction of crack propagation, which is similar to that observed on the specimen statically loaded in air, except that the environment might have altered some of the fine details on the ridges.

D. Dwell Fatigue

- Cracking occurred at the intersection of an inclined basal slip band with a $\{10\bar{1}7\}$ plane that was nearly perpendicular to the loading direction. The basal slip band was in a high resolved shear stress orientation (basal pole 42 deg from loading direction), whereas the preferred propagation planes were those in which maximum normal stress was resolved onto the $\{10\bar{1}7\}$ plane. Other irrational $\{hkil\}$ planes near $\{10\bar{1}7\}$ were also observed less frequently.

- The microscopic surface topography of these facets was consistent with that formed by static loading in air and 3.5 pct NaCl, suggesting that they have all formed by similar mechanisms and that the environment and unload/reload cycles act to modify the rate of crack propagation. Based on the time to failure of each specimen, loading in 3.5 pct NaCl seemed to increase crack growth rates substantially, whereas the addition of the unload/reload seemed to slow crack growth compared with the statically loaded specimens.
- The crystallographic plane of fracture was consistent with known hydride habit planes, and the fracture surface topography was consistent with facets formed in hydrogen gas atmosphere. The formation of fine tear ridges on the facet surface is consistent with localized softening caused by the hydrogen enhanced localized plasticity mechanism.
- Crack propagation rates within the faceted region were on the order of $2 \mu\text{m cycle}^{-1}$ at crack lengths between $20 \mu\text{m}$ and $100 \mu\text{m}$, which was considerably higher than those observed during continuous cycling. Because of the higher growth rates, the cracks grew preferentially through the faceted region before extending into the adjacent, differently oriented grains. This finding implies that the small crack growth regime may be equally as important to explaining the “dwell effect” as the crack-initiation stage. These accelerated crack growth rates are particularly detrimental in heavily microtextured material where there are similarly oriented basal planes affording an easy crack path.

ACKNOWLEDGMENTS

This work was funded partially by the Federal Aviation Administration (Grant 08-G-009) and the Office of Naval Research (Contract No. N00014-06-1-0089). One of the authors (A.L.P.) acknowledges support and encouragement of the Air Force Research Laboratory management and Air Force Contract No. FA8650-07-D-5800 during the preparation of this manuscript. The authors are also grateful to Dr. S. Fox (Timet, Henderson, NV) for providing the bar material used in this study and to Dr. A. Bhattacharjee (Defence Metallurgical Research Lab, Hyderabad, India) for his assistance with sample preparation and measuring the texture of the as-received bar. The authors appreciate the useful discussions related to fatigue and fracture of titanium alloys with Dr. M.C. Brandes (OSU) and the assistance of J. Foltz and A. Young (OSU) with electric discharge machining and stress corrosion cracking experiments, respectively. Finally, the authors would also like to acknowledge Dr. E. Medina and S. Putthanarat (Air Force Research Laboratory, Wright Patterson Air Force Base, OH) for performing the X-ray computed tomography investigation.

REFERENCES

1. L. Wagner, J.K. Gregory, A. Gysler, and G. Lütjering: *Proc. Second Eng. Found. Int. Conf./Workshop*, R.O. Ritchie and J. Lankford, eds., Santa Barbara, CA, 1986, pp. 117–27.
2. C.C. Wojcik, K.S. Chan, and D.A. Koss: *Acta Metall.*, 1988, vol. 36 (5), pp. 1261–70.
3. F. Bridier, P. Villechaise, and J. Mendez: *Acta Mater.*, 2005, vol. 53, pp. 555–67.
4. A.L. Pilchak, R.E.A. Williams, and J.C. Williams: *Metall. Mater. Trans. A*, 2010, vol. 41A, pp. 106–24.
5. J.E. Hack and G.R. Leverant: *Metall. Trans. A*, 1982, vol. 13A, pp. 1729–38.
6. W.J. Evans and M.R. Bache: *Int. J. Fatigue*, 1994, vol. 16 (7), pp. 443–52.
7. V. Sinha, M.J. Mills, and J.C. Williams: *J. Mater. Sci.*, 2007, vol. 42, pp. 8334–41.
8. V. Sinha, M.J. Mills, and J.C. Williams: *Metall. Mater. Trans. A*, 2006, vol. 37A (6), pp. 2015–26.
9. M.C. Brandes: Ph.D. Dissertation, The Ohio State University, Columbus, OH, 2008.
10. J.K. Gregory and H.-G. Brokmeier: *Mater. Sci. Eng. A*, 1995, vol. 203, pp. 365–72.
11. E. Richey and R.P. Gangloff: “Environmentally Assisted Cracking: Predictive Methods for Risk Assessment and Evaluation of Materials, Equipment, and Structures,” in *ASTM STP 1401*, R.D. Kane, ed., American Society for Testing and Materials, West Conshohocken, PA, 2000.
12. W.J. Evans: *Scripta Metall.*, 1987, vol. 21 (4), pp. 469–74.
13. M.R. Bache, H.M. Davies, and W.J. Evans: *Titanium '95: Science and Technology*, P.A. Blenkinsop, W.J. Evans, and H.M. Flower, eds., Institute of Materials, Birmingham, UK, 1996, pp. 1347–54.
14. M.R. Bache, W.J. Evans, and H.M. Davies: *J. Mater. Sci.*, 1997, vol. 32, pp. 3435–42.
15. M.R. Bache: *Int. J. Fatigue*, 2003, vol. 25, pp. 1079–87.
16. D.L. Davidson and D. Eylon: *Metall. Trans. A*, 1980, vol. 11A, pp. 837–43.
17. E. Uta, N. Gey, P. Bocher, M. Humbert, and J. Gilgert: *J. Microsc.*, 2009, vol. 233 (3), pp. 451–59.
18. B.F. Brown: *Stress Corrosion Cracking in High Strength Steels and in Titanium and Aluminum Alloys*, B.F. Brown, ed., Naval Research Lab, Washington, DC, 1972, pp. 1–16.
19. D.C. Slavik, J.A. Wert, and R.P. Gangloff: *J. Mater. Res.*, 1993, vol. 10, pp. 2482–91.
20. G. Themelis, S. Chikwembani, and J. Weerman: *Mater. Charact.*, 1990, vol. 24, pp. 27–40.
21. Y.J. Ro, S.R. Agnew, and R.P. Gangloff: *Scripta Mater.*, 2005, vol. 52, pp. 531–36.
22. N.E. Paton, J.C. Williams, J.C. Chesnutt, and A.W. Thompson: *Alloy Design for Fatigue and Fracture Resistance*, AGARD-CP-185, Technical Editing and Reproduction Ltd., London, UK, 1976, pp. 4-1–4-14.
23. J.C. Chesnutt, A.W. Thompson, and J.C. Williams: *Influence of Metallurgical Factors on the Fatigue Crack Growth Rate in Alpha-Beta Titanium Alloys*, Final Technical Report AFML-TR-78-68, 1978.
24. R.J.H. Wanhill, R. Galatolo, and C.E.W. Looije: *Int. J. Fatigue*, 1989, vol. 11 (6), pp. 4007–16.
25. F. McBagonluri, E. Akpan, C. Mercer, W. Shen, and W.O. Soboyejo: *Trans. ASME*, 2005, vol. 127, pp. 46–57.
26. F. McBagonluri, E. Akpan, C. Mercer, W. Shen, and W.O. Soboyejo: *Mater. Sci. Eng. A*, 2005, vol. 405, pp. 111–34.
27. A.L. Pilchak, A. Bhattacharjee, A.H. Rosenberger, and J.C. Williams: *Int. J. Fatigue*, 2009, vol. 31, pp. 989–94.
28. V. Sinha, J.W. Spowart, M.J. Mills, and J.C. Williams: *Metall. Mater. Trans. A*, 2006, vol. 37A, pp. 1507–18.
29. A.L. Pilchak, A. Bhattacharjee, R.E.A. Williams, and J.C. Williams: *Proc. 12th Int. Conf. Fracture*, CD proceedings, Ottawa, Canada, 2009.
30. A.L. Pilchak: Ph.D. Dissertation, The Ohio State University, Columbus, OH, 2009.
31. C.J. Szczepanski, S.K. Jha, J.M. Larsen, and J.W. Jones: *Metall. Mater. Trans. A*, 2008, vol. 39A, pp. 2841–51.
32. C.J. Szczepanski: Ph.D. Dissertation, The University of Michigan, Ann Arbor, Michigan, 2008.
33. J.C. Williams, R.G. Baggerly, and N.E. Paton: *Metall. Mater. Trans. A*, 2002, vol. 33A, pp. 837–50.
34. S. Suri, G.B. Viswanathan, T. Neeraj, D.-H. Hou, and M.J. Mills: *Acta Mater.*, 1999, vol. 47 (3), pp. 1019–34.
35. M.F. Savage, J. Tatalovich, and M.J. Mills: *Philos. Mag.*, 2004, vol. 84 (11), pp. 1127–54.
36. D.L. Davidson and J. Lankford: *Metall. Trans. A*, 1984, vol. 15A, pp. 1931–40.
37. T.L. Anderson: *Fracture Mechanics: Fundamentals and Applications*, 3rd ed., Taylor & Francis Group, Boca Raton, FL, 2005.
38. S. Suresh: *Fatigue of Materials*, 2nd ed., Cambridge University Press, New York, 1998.
39. J.V. Bernier, J.-S. Park, A.L. Pilchak, M.G. Glavicic, and M.P. Miller: *Metall. Mater. Trans. A*, 2008, vol. 39A, pp. 3120–33.
40. X.G. Zhang and J. Vereecken: *Corrosion*, 1990, vol. 46, pp. 136–41.
41. C.D. Beachem and R.M.N. Pelloux: *Fracture Toughness Testing and Its Applications*, *ASTM STP 381*, American Society for Testing and Materials, West Conshohocken, PA, 1965, pp. 210–45.
42. D.A. Meyn: *Metall. Trans.*, 1972, vol. 3A, pp. 2302–05.
43. C. Laird: *Fatigue Crack Propagation*, *ASTM STP 415*, American Society for Testing and Materials, West Conshohocken, PA, 1967, pp. 131–68.
44. A.P. Woodfield, M.D. Gorman, R.R. Corderman, J.A. Sutliff, and B. Yamrom: *Titanium '95: Science and Technology*, P.A. Blenkinsop, W.J. Evans, and H.M. Flower, eds., Institute of Materials, Birmingham, UK, 1996, pp. 1116–23.
45. A.P. Woodfield: GE Aviation, private communication, November, 2009.
46. V. Hasija, S. Ghosh, M.J. Mills, and D.S. Joseph: *Acta Mater.*, 2003, vol. 51, pp. 4533–49.
47. G. Venkataramani, D. Deka, and S. Ghosh: *Trans. ASME*, 2006, vol. 356 (128), pp. 356–65.
48. F.P.E. Dunne, A. Walker, and D. Rugg: *Proc. Royal Soc. A*, 2007, vol. 463, pp. 1467–89.
49. K. Kirane, S. Ghosh, M. Groeber, and A. Bhattacharjee: *J. Eng. Mater. Technol.*, 2009, vol. 131, pp. 021003-1–021003-14.
50. F.P.E. Dunne and D. Rugg: *Fatigue Fract. Eng. Mater. Struct.*, 2008, vol. 31, pp. 949–58.
51. M.C. Brandes, M.J. Mills, and J.C. Williams: *Metall. Mater. Trans. A*, in press. DOI: [10.1007/s11661-010-0407-z](https://doi.org/10.1007/s11661-010-0407-z).
52. J.S. Koehler: *Phys. Rev. B*, 1952, vol. 85, pp. 480–81.
53. D.S. Shih, I.M. Robertson, and H.K. Birnbaum: *Acta Metall.*, 1988, vol. 36, pp. 111–24.
54. P.E. Irving and C.J. Beevers: *Metall. Trans.*, 1971, vol. 2A, pp. 613–15.
55. J.C. Williams: *Effect of Hydrogen on Behavior of Materials*, A.W. Thompson and I.M. Bernstein, eds., Trans AIME, New York, NY, 1976, pp. 367–81.
56. J.D. Boyd: *Trans. ASM*, 1969, vol. 62, pp. 977–88.
57. A.R. Troiano: *Trans. ASM*, 1960, vol. 52, pp. 54–80.
58. I.M. Robertson and H.K. Birnbaum: *Proc. 11th International Conference on Fracture*, CD proceedings, <http://www.icf11.com/proceeding/EXTENDED/5759.pdf>, accessed 19 Dec 2009.
59. N.E. Paton and R.A. Spurling: *Metall. Trans. A*, 1969, vol. 7A, pp. 1769–74.
60. M.I. Luppò, A. Politi, and G. Vigna: *Acta Mater.*, 2005, vol. 53, pp. 4987–96.
61. X.H. Guo, S.Q. Shi, Q.M. Zhang, and X.Q. Ma: *J. Nucl. Mater.*, 2008, vol. 378, pp. 110–19.
62. M.R. Louthan: *Trans. Metall. Soc. AIME*, 1963, vol. 227, pp. 1166–70.
63. M.R. Louthan and R.P. Marshall: *J. Nucl. Mater.*, 1963, vol. 9, pp. 170–84.
64. R.N. Singh, R. Kishore, S.S. Singh, T.K. Sinha, and B.P. Kashyap: *J. Nucl. Mater.*, 2004, vol. 325, pp. 26–33.
65. A.R. Massih and L.O. Jernkvist: *Comp. Mater. Sci.*, 2009, vol. 46, pp. 1091–97.
66. M.-S. Yeh and J.-H. Huang: *Mater. Sci. Eng. A*, 1998, vol. 242, pp. 96–107.
67. R.H. Rusli: *Mater. Sci. Eng. A*, 2008, vol. 494, pp. 143–46.
68. A.W. Bowen: *Acta Metall.*, 1975, vol. 23 (11), pp. 1401–09.
69. W.J. Evans and C.R. Gostelow: *Metall. Trans. A*, 1979, vol. 10A, pp. 1837–46.

70. J.C. Chesnutt and N.E. Paton: *Titanium '80: Science and Technology, Proc. 4th World. Conf. on Titanium*, H. Kimura and O. Izumi, eds., Kyoto, Japan, 1981, pp. 1855–63.
71. A.W. Sommer and D. Eylon: *Metall. Trans.*, 1983, vol. 14A, pp. 2178–81.
72. W. Shen, A.B.O. Soboyejo, and W.O. Syeje: *Metall. Mater. Trans.*, 2004, vol. 35A, pp. 163–87.
73. W. Shen, W.O. Soboyejo, and A.B.O. Soboyejo: *Mech. Mater.*, 2004, vol. 36 (1–2), pp. 117–40.
74. A.A. Shaniavski and A.I. Losev: *Fatigue Fract. Eng. Mater. Struct.*, 2003, vol. 26 (4), pp. 329–42.
75. L. Toubal, P. Bocher, and A. Moreau: *Int. J. Fatigue*, 2009, vol. 31, pp. 601–05.
76. A. Bhattacharjee, D.M. Norfleet, M.J. Mills, and J.C. Williams, unpublished research, The Ohio State University, Columbus, OH, 2006 and 2009.
77. V. Sinha, R.B. Schwarz, M.J. Mills, and J.C. Williams: unpublished research, The Ohio State University, Columbus, OH, 2004.